UNIVERSIDAD NACIONAL AUTÓNOMA DE MÉXICO

POSGRADO EN CIENCIAS FÍSICAS

STATISTICS, DYNAMICS AND EFFECTIVE DEGREES OF FREEDOM OF COMPLEX SYSTEMS MODELS

TESIS

QUE PARA OBTENER EL GRADO DE

DOCTOR EN CIENCIAS (FÍSICA)

PRESENTA

ALVARO PATRICIO DÍAZ RUELAS

SUPERVISOR: DR. ALBERTO ROBLEDO
POSGRADO EN CIENCIAS F´ISICAS

CIUDAD DE MÉXICO, ENERO 2019

Contents

Part I

Prolegomena

Chapter 1

Introduction

Degrees of freedom of complex systems

A complete or integral idea of what statistical physics is about, can only be achieved if we disregard the central importance of thermal systems in the original construction of the field. Most realistic, complex systems, do not have an associated Hamiltonian. Still, ideas from statistical physics can be applied to them. It is for this reason that in this part of the work, we expose some of the basic mathematical concepts underlying the studies of general non-Hamiltonian and Hamiltonian systems, from which we study only examples of the non-Hamiltonian class.

The great problem with complex systems is that there is no such a thing as a general framework based on few principles, as for mechanical, either classical or quantum systems. Namely, the axiomatic formulation for classical mechanics due to D'Alembert, Lagrange, Laplace, Euler, Hamilton, Jacobi and others [1], or even better: Quantum mechanics, the most reliable physical theory we have up to now. For compactness, let's keep into the classical realm. According to the discipline of *analytical mechanics*, all what is needed for determining precisely the past and future of a mechanical system is the knowledge of the degrees of freedom of the system at some time of its evolution. This is a powerful statement that revolutionized science and boosted technology more than two centuries ago. Based on the success of this theory, Laplace famously wrote in *A Philosophical Essay on Probabilities* that someone with sufficient computational power ("Laplace's demon") could predict all past and future of the universe provided precise and complete knowledge of the mechanical state of all existing particles at a single time. Despite this theory being one of the most elegant creations of the human intelect, we now understand that this deterministic view is utterly reduced and impracticable for complex systems. Laplace's demon is an impossible construct. Nevertheless, in my point of view, this is one of the moments on the history of physics in which we see more clearly the important role that philosophy plays in scientific development. The classical studies of scientists like Joule, Kelvin, Carnot, Clausius and Helmhotlz on thermal systems opened the way to a new philosophycal perspective in which this determinism appeared to be insufficient. Thermal systems (simple substances, specially diluted gases) can be described by few degrees of freedom that can be measured in a macroscopic way, disregarding the microscopic nature of their huge number of constituent particles. This allowed Boltzmann [2], Maxwell, Gibbs [3] and others to propose a statistical interpretation of thermal phenomena. The success of this probabilistic view to mechanical systems gave birth to the exciting and wide discipline of Statistical Physics, which is itself endowed with dense philosophycal content. The solution to the central problem concerning physical irreversibility, the apparent natural unidirectional flow of time (at least for classical systems) is thought to be laying somewhere in the foundations of statistical

physics.
Thus, perhaps a revival on the proper use of philosphy in science is necessary to push the advancement on studies of complexity toward new horizons. There are some outstanding examples in which, at least in the technical realm, the boundary of complexity theory has being moved forward and reside mainly in the context of machine learning and the theory behind it. It is in the spirit exposed above that Lanczos wrote in *The variational principles of mechanics*:

> *In our day, we have witnessed at least one fundamental discovery of unprecedented magnitude, namely Einstein's theory of General Relativity, which was obtained by mathematical and philosophical speculation of the highest order.*

Therefore, a great portion of the problem lies on the successful identification of the relevant degrees of freedom, for each relevant scale, or even better, if possible, of the degrees of freedom useful for many or all the scales involved in generic problems. This is in general not known and thus a thermodynamic framework, at least in the classical sense, cannot be established. To this end, it would be necessary a sort of global formalism that construct local formalisms. Concerning this problem of scales, dynamics and statistics, in Part II we show how in a simple one-dimensional system with complex dynamics is
The great majority of 'systems' we study, or we are prone to study are curiosly more or less predefined by the ways they can be looked at. That's how we can call them systems in the first place, because there is some suggestion on their behavior that makes us think of observables that are well defined and measured, although they could hide a great complexity, due to not obvious or explicit degrees of freedom. Besides, what seems as 'well- defined' according to our perception, could be an amazingly intrincated combination of, actually simpler, variables. One example comes from biology. In ecology there exists the old problem of defining a proper measure of diversity of species in an ecological system [4]. Even defining what a species is represents a problem, but that is a wider discussion outside the scope of this work. For now, let us accept that there exist *ecological elements or objects*, *i.e.*, the species, which will take the place of the particles or elementary constituents of our ecologycal system. Making this abstraction is helpful for translating the problem into the language of physics and therefore, to try to reach some kind of statistical argument to treat the system macroscopically. Some models have been built based upon this approach, such as the one we address in Part III, which conforms a central portion of this Thesis.

Approaches to effective reduction of degrees of freedom

The usual practical approach when dealing with a complex problem, is to hope for the best when building a model for its description. This model must preferably be low dimensional and reduced in parameters, although high dimensional systems with many free parameters are commonplace. The physicist dream is to always be able of get rid of all the parameters and attain a suitable parameter-free description. As it happens, this is not the rule but the exception. Proteins, for instance, specifically the problem of protein folding, constitute a highly complicated problem that necessitates a complexity reduction. The thermodynamical and kinetic aspects of protein folding have been extensively studied [5] but a complete description of the dynamics of single proteins is out of reach due to the several and separated time scales involved, arising from the complex and numerous interactions between their constituent chemical groups, that are by themselves not simple units in general.

The so-called *theory of complex networks* is one tools preferre by the community for tackling real-world complex problems, ranging from human mobility to the workings of animal and human brains [6, 7]. The

success of this tools can be regarded as astonishing considering the wide range of applicability that the simplicity of the concept of what a network is allows. Almost everything that can be abstracted, can be fitted into the form of a network, and this in turns allows the application of the developed machinery up to know. Upon application of these machinery, one can truly find effective degrees of freedom in many-body systems, for many complex situations. These are, in my opinion, the main reason for which the community working under this approach grew so fast. But I think that the most sensible way to reach a new frontier in the understanding of complexity is not by the industrialized application of new tools without further thinking. I am not stating that the former works are unimportant, but a deep revision of all the rapid advances in empirical and technical terms could be performed and much understanding could be gained.

In Part IV I intend to put the different problems addressed in Parts II and III into the same perspective and try to give some humble philosophycal insights into bigger problems related to them. The author is aware that this piece of work is nothing but a very small contribution to the field of complexity, but also hopes to expand the ideas put here and to expand the boundary of understanding of these fascinating phenomena. Whether there exists or not a unifying theory behind complexity is not clear, but that philosophy and mathematics are needed to find the answer is out of the question.
In Part IV a summary and a brief discussion are presented, with the intention to close this work with a unified flavor and to highlight some open questions and perspectives that can be followed in further explorations.

Chapter 2

Ergodic Theory

Ergodic theory is, loosely speaking, the problem of finding invariant measures of generic dynamical systems. More formally, ergodic theory is the study of those transformations defined on a measure space that leave invariant the measure of all measurable subsets of the space [8], *i.e.*, the study of measure-preserving transformations that are also indecomposable.

From the foundational point of view, there is much more to the subject of ergodicity than only the basic and loose idea we are thaught in standard courses of statistical mechanics [9]. The typical definition of ergodicity states that *for an ergodic system, the ensemble average of any observable on the phase space is equal to its time average*

$$\lim_{T\to\infty}\frac{1}{T}\int_0^T f(\mathbf{x}(t))dt = \int f(\mathbf{x})d\Gamma, \tag{2.1}$$

where $\Gamma = \Gamma(\mathbf{x})$ is the *natural* measure of the phase space.
From the mathematical point of view, this definition is limited. The formal definition of ergodicity comes in the language of measure theory, to be briefly exposed in the next section.
It is by assuming this ergodicity of the dynamics of the system that the postulate of *equal a priori probabilities* of microstates is justified [10]. Some authors, like Hill [11] consider the ergodic property and the equal *a priori* probabilities assumption on the same footing and write them as different postulates.
The main critique to the postulate of ergodicity in Krylov's works [] to this approach to statistical mechanics is that, apart from being a property very hard to prove, almost no real system is actually expected to fulfill ergodicity.

Basics of measure theory

Given a set X we define a σ-algebra of susbsets of X as the collection $\mathscr{A}$ of subsets of X that fulfill the following properties [12]:

(i) $\emptyset \in \mathscr{A}$ and $X \in \mathscr{A}$,

(ii) $A \in \mathscr{A}$ implies $A^c \in \mathscr{A}$,

(iii) for any finite collection $A_1, \ldots, A_n$ of subsets in $\mathscr{A}$ we have that $\bigcup_{i=1}^n A_i \; in \mathscr{A}$.
The former condition can extend to countable additivity:

(iv) for any countable collection $\{A_i\}_{i\in\mathbb{N}}$ of sets in $\mathscr{A}$, we have $\bigcup_{i\in\mathbb{N}}^{n} A_i \in \mathscr{A}$.

Once the construction of a *sigma*-algebra is ready, we can properly define the concept of measure. A measure ν is a real-valued* set function that sends the sets $A \in \mathscr{A}$ to the extended reals, this is

$$\nu : \mathscr{A} \to \mathbb{R}^{+}, \tag{2.2}$$

for which the following properties must hold:

1 The measure ν is *additive* if

$$\nu\left(\bigcup_{i=1}^{n} A_i\right) = \sum_{i=1}^{n} \nu(A_i) \tag{2.3}$$

for any finite sequence $\{A_1,\ldots,A_n) \subset \mathscr{A}$ of pairwise disjoint sets such that their union is in $\mathscr{A}$.

2 The measure ν is *countably additive* or σ*-additive* if

$$\nu\left(\bigcup_{i=1}^{\infty} A_i\right) = \sum_{i=1}^{\infty} \nu(A_i), \tag{2.4}$$

for any countably collection $\{A_i) \subseteq \mathscr{A}$ of sets that are pairwise disjoint such that their union is still in $\mathscr{A}$.

The sets A that can be assigned a value of the measure unambiguously are called measurable. The triad $(X,\mathscr{A},\nu)$ thus defined is known as a measure space. If the measure is normalized, $\nu(X) = 1$, the triad is called a probability space. A measure ν is said to be *invariant* under f if the condition

$$\nu(f^{-1}(A)) = \nu(A) \tag{2.5}$$

for all sets $A \in \mathscr{A}$ [13]. Invariant measures are the central object of study in ergodic theory. This measures are important in the analysis of the asymptotic properties of generic dynamical systems and are fundamental in physics. If we consider de set $\mathscr{M}$ consisting of all the invariant measures that can be properly defined on $\mathscr{A}$, interesting questions arise about the structure of this set. In particular, the convexity of $\mathscr{M}$ can be demonstrated [14], and this allows for all the invariant measures on the σ-algebra to be decomposed in terms of the extreme points of $\mathscr{M}$. These extreme points $\eta \in \mathscr{M}$ are indecomposabe and receive the special name of *ergidic measures*. Let us state this separately in the following [15]:

Proposition 1 Let $f : X \to X$ be a measurable transformation and η be an f-invariant probability measure. The following statements are equivalent.

1. The system (f,μ) is ergodic.
2. For every invariant set $A \in \mathscr{A}$ we have that either $\eta(A) = 1$ or $\eta(A) = 0$.
3. Every invariant function is constant almost everywhere, that is, in a set of full measure.

With the definition above, we can now talk about ergodicity on much more rigurous ground.

*A measure can take also complex values, but we keep the exposition here in the real realm.

Frobenius-Perron operator and Radon-Nikodym theorem

Of central importance later in the discussion in Part II, Chapter 4, are the following resuts regarding the evolution of measures under the action of maps on the interval reduced to the action of a linear operator known as the Frobenius-Perron operator.
For a general transformation on a set X, $T : X \to X$, such that $T \in L^1(X, \mathscr{A}, \nu)$ (which do not need to be measure-preserving) its associated Frobenius-Perron operator $\mathscr{L}$ is defined through the integral relation

$$\int_A \mathscr{L}\rho d\nu = \int_{T^{-1}(A)} \rho d\nu, \tag{2.6}$$

for $A \in \mathscr{A}$ and $\rho \in L^1(X, \mathscr{A}, \nu)$. There is an interesting and fundamental probabilistic interpretation to the formula above. If we consider a random variable x on the probability space $(X, \mathscr{A}, \nu)$ has the corresponding probability density function $\rho(x)$, then the action of the transformation on this random variable $T(x)$, has the corresponding probability density function $\mathscr{L}\rho$. Let us define as μ the measure of the function of the density ρ under the preimage set $T^{-1}(A)$

$$\mu(A) = \int_{T^{-1}(A)} \rho d\nu, \tag{2.7}$$

then we can write the integral relation in Eq. (2.6) in the form

$$\mathscr{L}\rho = \frac{d}{d\nu}\mu. \tag{2.8}$$

The uniqueness of $\mathscr{L}$ is guaranteed by the application of a powerful, but relatively straightforward result known as the Radon-Nikodym theorem [16]:

> Assume that two σ-finite measures μ and ν are defined on a measurable space $(X, \mathscr{A})$. Furthermore, assume $\mu \ll \nu$ (μ is absolutely continuous with respecto to ν). Then there exists a measurable function $\rho : X \to [0, \infty)$, such that for any measurale set $A \subseteq X$,
>
> $$\mu(A) = \int_A \rho d\nu. \tag{2.9}$$

The function ρ is unique, and is known as the Radon-Nikodym derivative of μ with respect to ν. Hence, according to the above theorem $\mathscr{L}\rho$ in is a Radon-Nikodym derivative, which is unique for given μ and ν such that $\mu \ll \nu$. This last assumption of absolute continuity will be seen to be abandoned for the problem presented in Chapter 4, with important implications for our interests.

Coarse-grained measure

The characteristic function is a set function defined as

$$\begin{aligned} \chi(x) &= 1, \text{ if } x \in A \text{ or}, \\ &= 0, \text{ if } x \notin A \end{aligned} \tag{2.10}$$

now we can define the coarse-grained measure

$$\tilde{\rho}_i(x) = \sum_i \rho_i \frac{\chi_i(x)}{|\mathscr{M}_i|} \tag{2.11}$$

where

$$\rho_i = \int_{\mathscr{M}_i} dx \rho(x) \tag{2.12}$$

is the piecewise constant density over the partition over regions $\mathscr{M}_i$ that coarse-grains the space. Now let us evolve this measure one unit of time by applying the Frobenius-Perron operator once

$$\begin{aligned} \rho_i' = \mathscr{L} \cdot \rho_i &= \int_{\mathscr{M}_i} dx (\mathscr{L} \cdot \rho)(x) \\ &= \int_{\mathscr{M}_i} dx \int dy \rho(y) \delta(x - f(y)) \\ &= \sum_j \rho_j \frac{\chi_j(x)}{|\mathscr{M}_j|} \int_{\mathscr{M}_i} dx \int_{\mathscr{M}_j} dy \delta(x - f(y)) \end{aligned} \tag{2.13}$$

we can identify the double integral above as the quotient

$$\int_{\mathscr{M}_i} dx \int_{\mathscr{M}_j} dy \delta(x - f(y)) = |\mathscr{M}_i \bigcap f^{-1}(\mathscr{M}_j)| \tag{2.14}$$

which, by inserting it into last line of Eq. (2.14) corresponds to the elements of the matrix representation of the approximate Frobenius-Perron operator

$$L_{ij} = \frac{|\mathscr{M}_i \bigcap f^{-1}(\mathscr{M}_j)|}{|\mathscr{M}_i|}. \tag{2.15}$$

Hence, Eq. (2.14) can be written as

$$\rho_i' = \sum_j L_{ij} \rho_j \frac{\chi_j(x)}{|\mathscr{M}_j|}, \tag{2.16}$$

or as

$$\rho' = \rho \mathbf{L}. \tag{2.17}$$

In the one dimensional case we are going to address, this treatment coincides with the histogram of the evolution of an ensemble.

Chapter 3

Piecewise monotone maps of the interval

Theorems and general properties

In the following, we denote by $\mathbf{C}$ as the set of continuos functions on the interval $I \in \mathbb{R}$, $I = [a,b]$. We are interested in the class of all piecewise monotone mappings $\mathbf{M}$, $\mathbf{M} \subset \mathbf{C}$. We will analyze the dynamics of functions $f : I \to I$ such that $f \in \mathbf{M}$. This class of mappings has the advantage that the theorems we will use apply to any member of $\mathbf{M}$. A mapping is said to be piecewise monotone if there exists a partition f the interval $a = l_0 < l_1 < \ldots < l_N < l_{N+1} = b$ such that f is strictly monotone on $[l_k, l_{k+1})$ for each $k = 0, \ldots, N$. The points u in which f is not monotone in any neighborhood of u are called turning points. The usual question that arises around this class of mappings is about the asymptotic behavior of their orbits, this is $\{f^n(x)\}_{n\to\infty}$ for typical initial points. Piecewise monotone maps of the interval have been deeply studied as suitable qualitative models of real processes since works such as May's well-known *Simple mathematical models with very complicated dynamics* [17]. Despite decades have past since the beggining of these studies, active mathematical research it is being done with respect to one-dimensional dynamics [18].

The main matter I want to expose here is a general result, Theorem 2.4 in [19]. This theorem tells us about the behavior of typical orbits (in the topological sense) of mappings $f \in \mathbf{M}$. According to this result, these typical orbits can only get one three different kinds of asympotic behavior, namely:

(i) The destiny of the orbit is an f-invariant subset $C \subset I$, which consists of finitely many closed intervals, on wich f has an action that is topologically transitive. Topological transitivity means that the orbit of some point in C is dense in C.

(ii) There is a Cantor-like set R, invariant under f to which the orbit is attracted and acts *minimally* on it. The implication of this is that each of the orbits on R set are dense on R.

(iii) An f-invariant open set $Z \subset I$ contains the orbit. Also, all the compositions f^n, $n \geq 0$ are monotone in the connected components of Z

The former is a strong result that classifies the dynamics in a stringent way. There is the other part of the story, which is about the structure of the subset on the interval for which none of the above conditions are true. Despite being a small set, it is important because it can influence the global complexity of the iterates of f. In this work, point (ii) is the main reason leading to the complexity of the iterates of the map we analyze.

The behavior of long-term iterates of dynamical systems close to transitions from periodic to chaotic motion has been an active and fruitful subject of study for decades [20]. Nevertheless, the studies of the intricate nature of the transients of individual trajectories approaching the onset of chaos via different routes have proven to be of value for advancing in the understanding of the possible valid formulations of statistical mechanics for systems out of thermodynamic equilibrium [21]. Specifically, the interest has been put into the detailed transient phase of single trajectories, as well as ensembles of them, with initial conditions in successive steps of the period-doubling route to chaos of the logistic map, as well as in the accumulation point of this cascade. The form of the logistic map we use is the following

$$f(x) = 1 - \mu x^{|z|},\ x \in [-1,1],\ \mu \in [0,2] \tag{3.1}$$

with quadratic maximum, $z = 2$. From the thorough analysis of the dynamics of trayectories at successive steps in the period-doubling cascade, it has been demonstrated [22] that the dynamics at the transition point, the Feigenbaum point, is approximated with increasing similarity by the transient dynamics of trajectories initiated at each of the steps of the bifurcation cascade as the accumulation point is approached. In [22,23] it is described how a deformed statistical-mechanical structure emerges from the aforementioned connection between the transient dynamics (via the succession of superstable cycles) and the dynamics at the Feigenbaum point ($\mu = \mu_\infty$). The whole description of the intricate dynamics of approach of single trajectories to periodic, superstable attractors in the succession of period doublings is shown in full detail in [22]. In the same spirit, but on the problem of revealing the statistical nature of the onset of chaos, work has been done via the detailed analysis of the sums of iterates of nonlinear low dimensional maps, obtaining interesting implications to the possible generalizations of the CLT for correlated variables describing nonequilibrium processes [24–27], only to mention one of those. Nevertheless, despite this statistical analysis, no work has been done concerning the matter of nonuniform convergence of the distributions at the Feigenbaum point.

Part II

Probabilistic and statistical approaches

Chapter 4

Fokker-Planck equation and Frobenius-Perron operator

As an additional example of succesful reduction of degrees of feedom in a model (although this effective behavior is different in nature), in this section we study the evolution of the density of iterates of the logistic map at a representative set of dynamical regimes: From the periodic motion at superstable orbits of the period-doubling route to chaos and its corresponding, aperiodic, accumulation point; to the chaotic motion at Misiurewicz points, along the band-splitting chaotic cascade. We restate the problem of studying individual orbits of the logistic map and change the picture to ensembles of positions evolving under the action of a linear operator acting on the density of iterations, in close resemblance to the classical normal diffusion problem, in which the problem of tracking the dynamics of single particles via the Langevin equations for each particle, can be recast into a single partial differential equation for the evolution of the probability density of finding a particle at a specific position and time, i.e., the Fokker-Planck equation. We have characterized in detail the evolution of the density of iterates in the phase space originated by the action of the Frobenius-Perron (FP) operator. It is found how a separation of time scales emerges; the dynamics underlying the evolution of individual trajectories on the time scale of single iterations of the map becomes, asymptotically, a larger time scale, if the condition that the density be invariant under the action of the FP operator is imposed. This time scales are exponentially separated: iterations follow the scale t, while $\tau \sim 2^n$ are the times for which the action of the FP dynamics is invariant, independently of the initial distribution of points in phase space. To be clear, the asymptotic distribution will almost always be different for different initial distributions but it will be invariant under the FP operator at times τ. The scaling of the density over this induced time scale τ is found to follow a renormalization-group (RG) structure. The entropy associated with evolving and invariant densities via the Shannon expression has extrema at the fixed points of the proposed RG operation. It is found that this entropy as a function of the control parameter has the behavior of an equation of state of a thermal system on a phase transition. This formalism summarizes in a novel and compact fashion many of the ideas exposed in previous works [21, 22] and opens the way to new insights by allowing the direct application of our RG-entropy approach and the complete formalism of thermodynamics.

Introduction

In Section 4.2 we study the approach of an ensemble of trajectories at successive bifurcation points and at the onset of chaos; then we calculate its associated densities of iterates. We show the emergence of a larger time scale, of the form $\tau = 2^n$ (where n is the order of the superstable orbit in the period-doubling sequence). Then we look at the scaling of those densities as the Feigenbaum point is approached through superstable cycles.
In Section 4.3 we study the band splitting process also in terms of the distributions of iterates at the well-defined sequence of Misiurewicz points. At this sequence of points, the dynamics is chaotic and the (expected) long time behavior of the density to be stationary. We confirm this stationary character in the larger time scale $\tau = 2^n$. These results are used in parallel to a rescaling scheme over the smooth, invariant distribution at $\mu = 2$, known as the Ulam density. This self-affine transformation on the Ulam distribution sequentially reproduces the band-splitting process at Misiurewicz points in an exact way, on the τ time scale. The convergence of the original smooth and 'regular' Ulam distribution toward a singular one with fractal support at the Feigenbaum point is found to be equivalent to that obtained for the period-doubling cascade. This contributes to the understanding of the convergence problem adressed in several works [28, 29], concerning possible generalizations of the CLT, mentioned earlier. The 'forward' cascade of period-doubling bifurcations meets the band-splitting cascade at the Feigenbaum point, and thus, both sequences of rescalings of disutributions are convergent at this point. This is supported here by numerical evidence and the treatment with the entropies.
Finally, in Sec.4.4 we propose a renormalization group (RG) scheme to the former prescription and describe the flow for the action of the RG transformation in parameter space. We conclude once more that the Feigenbaum point has a nontrivial fixed point distribution associated to it with respect to some suitable RG transformation and that the entropy extrema are reached at fixed points of this RG transformation [21].

Fokker-Planck equation for the logistic map

Here we obtain the analogous of a Fokker-Planck equation from a piecewise monotone map of the interval. This way we change the perspective of analysis we have followed in past works [21, 22], based on single trayectories, with or without the influence of noise, analogous to the Langevin approach in the classsical diffusion problem. To this end we switch to the point of view of ensembles of iterations, represented by densities on the interval. Later we show that this approach is indeed contained as a special case into the general theory of ergodicity. Starting with the logistic map

$$x_{i,t} = 1 - \mu x_{i,t-1}^2, \;\; x_{i,t} \in [-1,1], \; t = 0,1,2\ldots \tag{4.1}$$

that would be the equivalent to the Lagrangian view, in coordinates $x_i(t)$ in fluid flow analysis in which one follows a the trajectory of a single particle in time. Thus, in order to get the overall picture we pass to Eulerian coordinates x. We may write

$$p(x,t) = \int \mathrm{d}x' p(x,t|x',t-1) p(x',t-1) \tag{4.2}$$

with $x = 1 - \mu x'^2$. In this case, the conditional transition probability is given by a Dirac delta

$$p(x,t|x',t-1) = \delta(x - 1 + \mu x'^2) \tag{4.3}$$

Hence we get the expression

$$p(x,t) = \int_{-1}^{1} \mathrm{d}x' \delta(x-1+\mu x'^2) p(x',t-1), \tag{4.4}$$

that, after the change of variables $y = 1-\mu x'^2$ for $x' \in [0,1]$ and $z = 1-\mu x'^2$ for $x' \in [-1,0]$ becomes

$$p(x,t) = \frac{1}{2\sqrt{\mu(1-x)}} \left[p\left(\sqrt{\frac{1-x}{\mu}}, t-1\right) + p\left(-\sqrt{\frac{1-x}{\mu}}, t-1\right) \right] \tag{4.5}$$

for $x \in [1-\mu, 1]$ and $p(x,t) = 0$ for $x \in (-1, 1-\mu)$. We will derive this same equation from a different but equivalent approach in the next section.
There is an important difference between the Fokker-Planck equation and the equation we obtained for the logistic map, Eq. (4.13), and this is that the inverse of the logistic map is not unique. Therefore, the "backwards" equation of Eq. (4.13), analogous to reverse time in the Fokker-Planck equation, is obtained by inserting in Eq.(4.6) the backward propagation of the probability density

$$p(x,t-1) = \int_{1-\mu}^{1} \mathrm{d}x' p(x,t-1|x',t) p(x',t) \tag{4.6}$$

with $x = \pm\sqrt{\frac{1-x'}{\mu}}$. The conditional transition probability is a sum of two Dirac deltas

$$p(x,t-1|x',t) = \frac{1}{2}\delta\left(x - \sqrt{\frac{1-x'}{\mu}}\right) + \frac{1}{2}\delta\left(x - \sqrt{\frac{1-x'}{\mu}}\right) \tag{4.7}$$

Hence we have the expression

$$p(x,t-1) = \int_{-1}^{1} \mathrm{d}x' \left[\frac{1}{2}\delta\left(x - \sqrt{\frac{1-x'}{\mu}}\right) + \frac{1}{2}\delta\left(x - \sqrt{\frac{1-x'}{\mu}}\right) \right] p(x',t) \tag{4.8}$$

that yields

$$p(x,t-1) = \begin{cases} \mu x p(1-\mu x^2, t), & x \in [0,1] \\ -\mu x p(1-\mu x^2, t), & x \in [-1,0] \end{cases} \tag{4.9}$$

which is already normalized.

Transient and invariant densities of iterates for superstable orbits

The density of iterates at time t, $\rho_t(x)$, can be constructed also directly from the evolution of an initial density under the action of the map, by means of an operational approach. For an arbitrary initial density $\rho_0(x)$ of iterates distributed over the whole iterval I, provided the initial number of trajectories is preserved, the following must hold

$$\int_{f^t(I)} \rho_t(x) dx = \int_I \rho_0(x) dx$$

where I as total lebesgue measure m, hence $x_0 \in I$

Consider an arbitrary initial density $\rho_0(x)$ put to evolve in discrete time $\rho_t(x)$. Provided the relation above is valid for the dissipaive case [16, 30], we can think of a linear operator acting on arbitrary densities in phase space and pushing them forward in time. This operator is defined by the action

$$\rho_t(x) = \mathscr{L}^t \rho_0(x), \tag{4.10}$$

which is, in explicit form

$$\rho_t(x) = \int_I \delta[y - f^t(x_0)]\rho_0(y)dy \tag{4.11}$$

The above equation is known as the Frobenius-Perron equation and the associated linear operator pushing the density in time, as the Frobenius-Perron operator, with its singular kernel $\delta[y - f^t(x_0)]$ [30]. Notice that we have a linear relation between the delta-densities through the integral operation, despite the evolution law $f(x)$ for single trayectories being nonlinear.
From the Frobenius-Perron equation (Eq. (4.11)) we will get the invariant density of iterates in the phase space for the logistic map at different dynamical regimes, corresponding these to different phase-space mixing conditions. In this section, we focus on superstable attractors of the logistic map, Eq.(4.1), also known as supercycles. This subsequence of control parameter values will be denoted here as S_k, $k = 1, 2, 3, \ldots$, so 2^k gives the period of the superstable attractor in turn.

Evolution of the density along the period-doubling cascade.

The periodic superstable attractors form a sequence of points in the cascade of the period-doubling route to chaos with interesting dynamical and statistical propertiers properties [22, 23]. For one dimensional quadratic maps, the condition of a periodic point x^* being a critical point of the map, *i.e.* $f'(x^*) = 0$, is sufficient (and necessary) to guarantee stability of the orbit at a super-exponential rate. Hence, this condition defines the sequence of control parameter values we will use in the following, the so-called superstable orbits or supercycles.

Now we proceed to solve Eq. (4.11) explicitly for the logistic map, as defined by Eq. (3.1), at subsequent times

$$\rho_{t+1}(x) = \int_{I_0} \delta[y - 1 + \mu x^2]\rho_t(y)dy \tag{4.12}$$

with I_0 the initial set representing an ensemble of positions, to be considered as the interval $[-1, 1]$ with full Lebesgue measure and uniform density. Integration of the above expression yields

$$\rho_{t+1}(x) = \frac{1}{2\sqrt{\mu(1-x)}}\left[\rho_t\left(\sqrt{\frac{1-x}{\mu}}\right) + \rho_t\left(-\sqrt{\frac{1-x}{\mu}}\right)\right] \tag{4.13}$$

for $x \in [1-\mu, 1]$ and $\rho_t(x) = 0$ for $x \in (-1, 1-\mu)$. Eq. (4.13) is properly normalized as it stands. As we showed in previous section, Eq. (4.13), is a discrete-time analog of the Fokker-Planck equation in condensed matter theory, but for a particular dynamical system which is continuos in space and discrete in time. This equation is valid for subsequent times, but we are also interested in the asymptotic state of the dynamics of the density.
Relying on numerical evidence (See Fig. 4.1), we give support to the conjecture that the invariant distribution corresponding to the asymptotic state of the successive compositions of the Frobenius-Perron

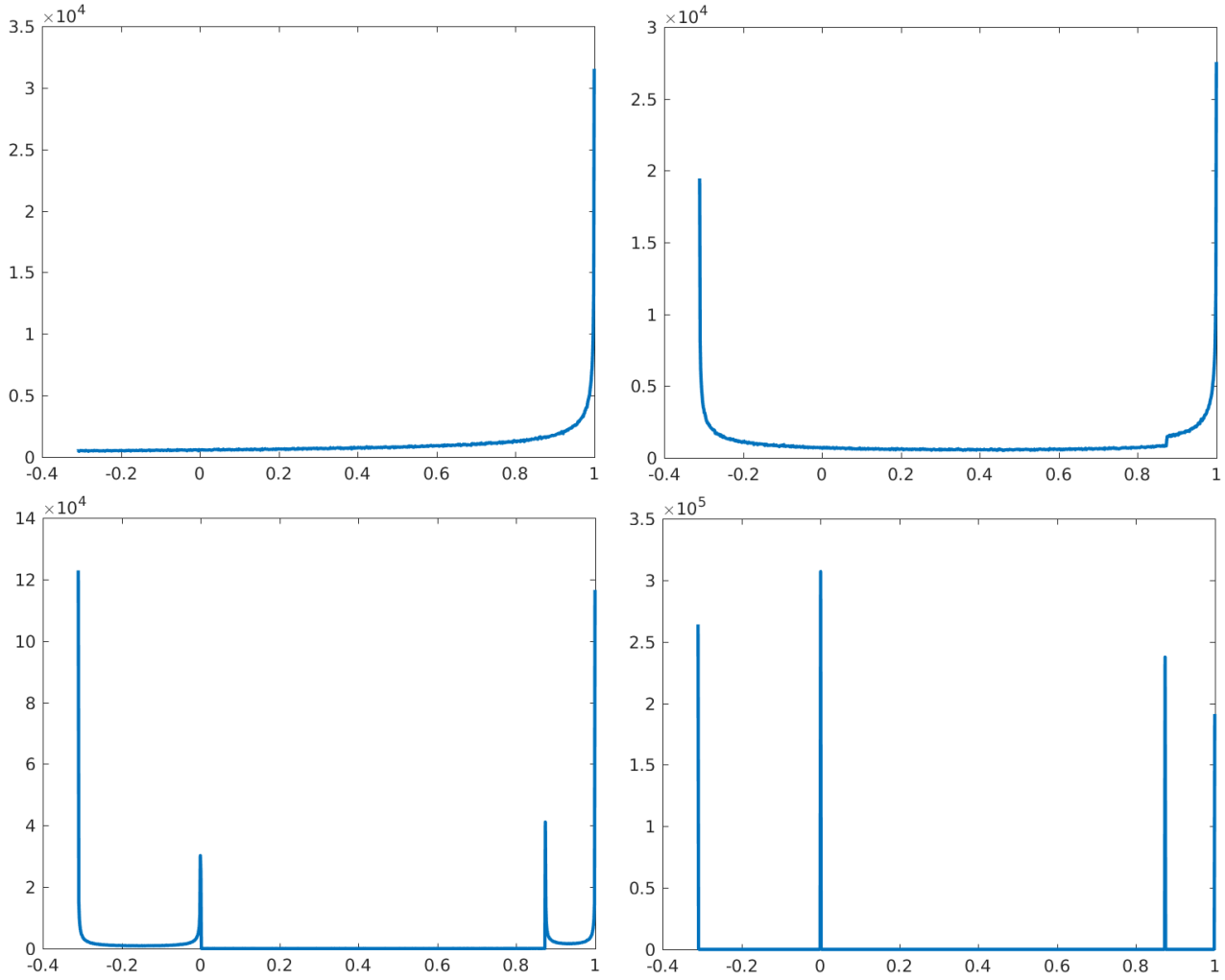

Figure 4.1: Evolution of an initially uniform density of positions in the interval $[-1,1]$. Panel (a) At the first iteration, the density tends to accumulate around one, which confirms the findings described in [22]. Panel (b) corresponds to the second iteration of the initial uniform density under the action of the map. Notice the formation of a peak around -0.3. In Panel (c) we see the result of ten iterations of the Frobenius-Perron operator, where we can see four peaks centered on the final attractor points: $\{\sim -0.31, 0, \sim 0.87, 1\}$. These attractor points are clearly noticeable in Panel (d) where the to the long term state (about 5000 iterations, in this case) of the density under the action of the PF operator is presented.

operator, for an initial arbitrary density at superstable, periodic regimes ($\mu < \mu_\infty$) is a distribution whose support is the interval $[-1,1]$ on its way to become a fractal set. Hence we write

$$\mathscr{L}_\mu^\infty[\rho_0(x)] = \sum_{k=0}^{2^n-1} A_k \delta(x - x_k^*), \tag{4.14}$$

where the A_k's are the 'intensities' of the deltas and the subindices of the positions x_k^* follow the order given by the dynamics of the attractor points. The expected natural measure for a system on a periodic regime of period p is given by [15]

$$\nu_p = \frac{1}{p}\sum_{j=0}^{p-1}\delta(f^j(x)-x^*). \tag{4.15}$$

Provided that the measures ν_p are ergodic, equations (4.14) and (4.15) would be equivalent. This means that $A_k = A = 1/p$. Nevertheless, this is not the numerical result. In rigurous terms, the reason is that the measure obtained from the Frobenius-Perron evolution is not ergodic. Considering the numerical results alone, this can be understood by the finite precision, finite iteration time, the different local scaling constants and, more importantly perhaps, the fractal structure of the unstable repeling positions which make the orbits coming from different region to have exponentially different arrival times to attracting positions. This fractal structure and the so-called times of flight of the positions is addressed in [22]. The set of repelling positions (also a set of measure zero with respect to the Lebesgue measure) accumulates no density; actually, it is clear that the density is zero at these points. That nonergodic character is precisely the problem with these measures, obtained for $\mu < \mu_\infty$ is that they are not absolutely continuous with respect to the Lebesgue measure. This implies that the sets of zero Lebesgue measure are not necessarily of measure zero under ν. In fact, they are not in our case, as the set of periodic points accumulate all the ν-measure. Hence, averages over ν carry a different physical meaning than those performed over m. We are working on a way to 'regularize' the measure obtained at μ_∞ so physiscal meaning can be extracted from averages over it.

The first superstable attractor (denoted here as S_1), corresponding to control parameter value $\mu_1 = 1$, is composed by two fixed points, namely, the positions $x_0^* = 0$ and $x_1^* = 1$. By the mere defining characteristic of the superstable attractors, the former two points are members of the attractor set for all values of k even in the limit $k \to \infty$. For instance, the expected 'invariant' distribution at some 'post-transient' time is, for S_2 ($\mu_2 = 1.3107026413368...$)

$$\rho_{S_2}(x) = A_0\delta(x-x_0^*) + A_1\delta(x-x_1^*) + A_2\delta(x-x_2^*) + A_3\delta(x-x_3^*) \tag{4.16}$$

Taking $\rho_t(x) = \rho_{S_2}$ in the right side of Eq. (4.13), and considering that the singular density cannot be symmetric, so $\rho\left(-\sqrt{\frac{1-x}{\mu}}\right) = 0$ necessarily, we get

$$\rho_{t+1,S_2}(x) = A_0\delta(x-x_1^*) + A_1\delta(x-x_2^*) + A_2\delta(x-x_3^*) + A_3\delta(x-x_0^*). \tag{4.17}$$

This means that the locations of the densities have just cycled over the fixed points conforming the attractor. This can be seen clearly in Fig. 4.2. We adopt the convention that the 'zero time' just after the transient dynamics is when the density at $x_0^* = 0$ corresponds to the lowest peak (lowest A_k). Hence, in general, for the forward application of Eq. (4.13) to $\rho_{S_n}(x)$ we have

$$\mathscr{L}\left[\sum_{k=0}^{2^n-1} A_k\delta(x-x_k^*)\right] = \sum_{k=0}^{2^n-1} A_k\delta(x-x_{\sigma(k)}^*) \tag{4.18}$$

with the property

$$\mathscr{L}^{2^n}\left[\sum_{k=0}^{2^n-1} A_k\delta(x-x_k^*)\right] = \sum_{k=0}^{2^n-1} A_k\delta(x-x_k^*), \tag{4.19}$$

where $\sigma(k)$ in Eq. (4.18) pushes the index by one unit, according to the dynamics of the map, this is, $\sigma(k) \to k+1$, $k \neq 2^n$ and $\sigma(2^n-1) \to 0$, therefore $\sigma^{2^n}(k) = k$. From the former property we see the emergence of two distinct time scales. The one associated to the single action of the Frobenius-Perron

operator, Eq. (4.11), which is tied to the dynamics of the compositions of the map, as it can be seen from the kernel $\delta[y - f^t(x_0)]$ of the Frobenius-Perron operator. This time scale is represented by the index k or t. The second, largest, time scale is 'parametrized' by n so it depends on the dynamical regime. It is formed by steps of $\tau = 2^n$, hence it increases exponentially with respect to the 'natural' scale given by the Frobenius-Perron dynamics.

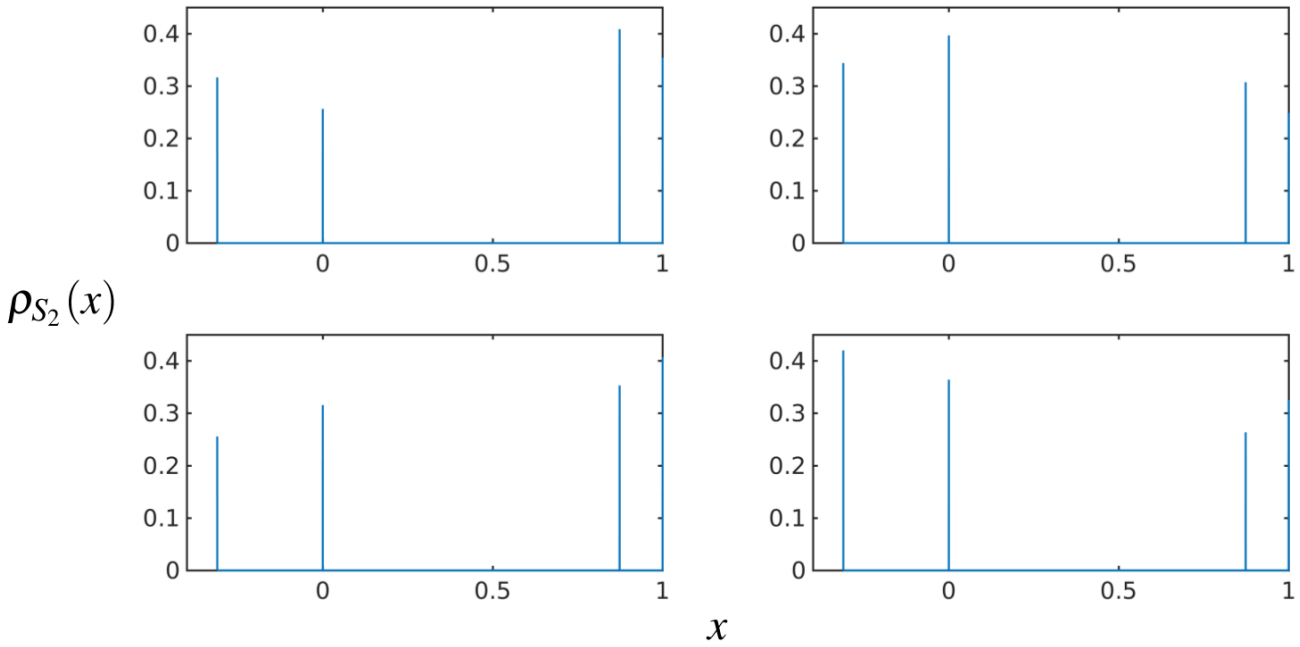

Figure 4.2: In the upper left panel the density at $t = T$ (by convention) is depicted. It can be clearly seen how the density peaks cycle over the attractor points without changing at all in magnitude. This cycling is given by the same dynamics of the fixed points x_k forming the attractor.

Density of iterates at the Feigenbaum point.

The accumulation point of the bifurcation cascade is reached as $n \to \infty$. Here motion becomes aperiodic, hence Eq. (**??**) would read

$$\lim_{n\to\infty} \mathscr{L}^n_{\mu_\infty}[\rho_0(x)] = \sum_{k=0}^{2^n-1} A_k \delta(x - x^*_k),$$

Nevertheless, convergence to the above limit is not guaranteed, because there is not absolute continuity with respect to the initial Lebesgue measure. Indeed, due to the condition of absolutely continuous condition imposed for uniqueness of the Frobenius-Perron operator, one would rather expect that limit to be zero. This tell us that in the limit $n \to \infty$ at the Feigenbaum point, one could probably not be able to define a Frobenius-Perron unambiguously. But due to the ergodic theorem, we know that a density can be asigned to this sets, so we conjecture that for the asymptotic limit of the application of the Frobenius-Perron operator, the condition of absolute continuity is lost.
Therefore, we have to introduce another notion, expressed by the relation

$$\mathscr{L}_{\mu}^{T}[\rho_0(x)] = \sum_{k=0}^{2^n-1} A_k \delta(x - x_k^*),$$

where T represents a long iteration time, but still not the infinite limit. This can be interpreted as an intermediate 'quasi-stable' state of the Frobenius-Perron dynamics on piecewise monotone functions on the interval for which the behavior (ii) exposed in Sec. 3.1 holds. Furthermore, an imporant implication of the stability of the quantity in Eq. 4.2 is that there exist a level of coarse graining for which the T-th application of the Frobenius-Perron operator has an eigenfunction. We think these are important findings that deserve further studies.

Transient and invariant densities at Misiurewicz points.

We will now focus our attention on a sequence of points in the chaotic regime $\mu > \mu_\infty$, particularly the sequence of control parameter values where the chaotic bands are about to split, known as Misiurewicz points. This band-splitting scenario is the chaotic equivalent to the period-doubling scenario for $\mu < \mu_\infty$ studied in Sec. 4.2. The points $\{x_b\} \in [-1,1]$ that correspond to the borders of the bands at Misiurewicz points are well defined by positions of the the trajectory initiated at zero, *i.e.* $x_{b_{n+1}} = f(x_{b_n})$, $x_{b_1} = 0$.

Invariant Measure as a stationary solution.

In this case, Eq. (4.11) is also valid. We obtain the successive densities (believed to be stationary) at the sequence of Misiurewicz points.
For $x \in [1-\mu, 1]$ we look for the stationary solution $\rho_t(x) = \rho_{t+1}(x)$ of Eq. (4.13). This solution, that we will call ρ_{eq} must satisfy

$$\rho_{\text{eq}}(x) = \frac{1}{2\sqrt{\mu(1-x)}} \left[\rho_{\text{eq}}\left(\sqrt{\frac{1-x}{\mu}} \right) + \rho_{\text{eq}}\left(-\sqrt{\frac{1-x}{\mu}} \right) \right]. \tag{4.20}$$

We test the invariant density of iterates of the logistic map in the fully chaotic regime, also known as the Ulam map $f(x) = 1 - 2x^2$ under this developed framework. First noticing that the corresponding density $(\rho(x), p(x))$ of the Ulam map

$$\rho_{\text{eq}} = \frac{1}{\pi\sqrt{1-x^2}} \tag{4.21}$$

is symmetric around zero

$$\rho_{\text{eq}}(-x) = \rho_{\text{eq}}(x)$$

with this, Eq. (4.20) becomes

$$\rho_{\text{eq}}(x) = \frac{\rho_{\text{eq}}\left(\sqrt{\frac{1-x}{\mu}}\right)}{\sqrt{\mu(1-x)}} \tag{4.22}$$

it can be easily verified that the density defined by Eq. (4.21) indeed fulfils Eq. (4.22).

Scaling of the invariant measure at Misiurewicz points

The invariant density of the iterates of the logistic map with $z = 2$ also referred to as the Ulam map, is given by the well known expression already presented in Eq. (4.21)*

$$p(x) = \frac{1}{\pi\sqrt{1-x^2}} \tag{4.23}$$

Next, we show how at the Misiurewicz points the invariant distribution can be obtained by proper scalings of Eq. (4.23). Let us consider the first Misiurewicz point. Passing to the variable

$$y \equiv bx + a,\ 0 < b < 1,\ -1 + b < a < 1 - b$$

we have

$$\begin{aligned} \rho_Y(y) &= \int \mathrm{d}x \rho_X(x)\delta(y - bx - a) \\ &= \frac{1}{b}\rho_X\left(\frac{y-a}{b}\right), \end{aligned} \tag{4.24}$$

we thus obtain

$$\rho(x) = \frac{1}{\pi\sqrt{b^2 - (x-a)^2}}. \tag{4.25}$$

So, at the first Misiurewicz point the scaling ansatz gives

$$\rho(x) = \begin{cases} \left(2\pi\sqrt{b_1^2 - (x-a_1)^2}\right)^{-1}, & x \in [-b_1 + a_1, b_1 + a_1] \\ \left(2\pi\sqrt{b_1^2 - (x-a_2)^2}\right)^{-1}, & x \in [-b_2 + a_2, b_2 + a_2] \end{cases} \tag{4.26}$$

with $-1 + b_1 < a_1 < 1 - b_1$, and $a_2 = a_1 + b_1 + b_2$ or $a_2 = a_1 - b_1 - b_2$.

Following this procedure, we get the expression for the densities at each Misiurewicz point as the Feigenbaum attractor is approached with $k \to \infty$

$$\rho_{M_k} = \frac{1}{2^{k+1}\pi\sqrt{b^{2(k+1)} - (x - (k+1)a)^2}} \tag{4.27}$$

In the equation above, we can notice that $b^{2(k+1)} \to 0$ as $k \to \infty$. But that would mean ρ_{M_k} become a complex quantity unless the inequality

$$b^{2(k+1)} \geq (x - (k+1)a)^2 \tag{4.28}$$

is strictly satisfied as $k \to \infty$. This implies also that $x - (k+1)a \geq 0$ on each corresponding region (band). This indicates that there exists a tight relationship between the constants a, b and the universal scaling constants α and δ. This is also work in progress.

*The perhaps more widespread expression is $p(x) = 1/\pi\sqrt{x(1-x)}$, but that corresponds to the form of the logistic map given by $f(x) = ax(1-x)$.

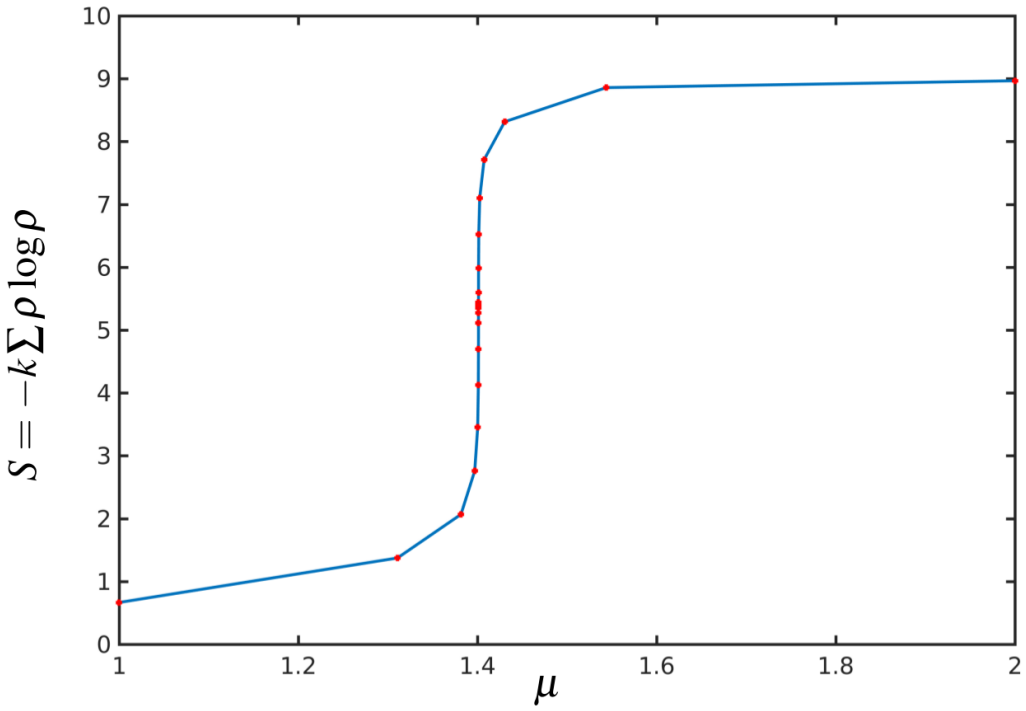

Figure 4.3: Entropy vs control parameter value. NOTES: Zoom into the region around $\mu = \mu_\infty$, preferably

Renormalization Group approach to the Frobenius-Perron Dynamics

The renormalization scheme operating at the level of the invariant distributions at Misiurewicz points has a straightforward geometric visualization. Take the horizontal axis in Fig. and then cut the final group of density peaks, corresponding to the region close to $x = 1$, after this, stretch the x axis accordingly to recover the.

After this operation, which will retain the normalization and stretch the x axis.

From the calculation of Shannon entropy for the numerically calculated densities at each superstable and Misiurewicz point, we get an interesting result. Namely, that the logistic map on its route to chaos by period-doubling along with the band splitting scenario out of chaos, can be viewed as a macroscopic system in equilibrium undergoing a phase transition.

In Fig. 4.3 it is seen how a phase separation occurs similar to the spontaneous magnetization displayed by a magnet below its Curie temperature, here representing a transition between two distinctive behaviors: the regular motion associated to the period-doubling cascade, followed by a phase transition at constant temperature, *i.e*, control parameter value μ, in which entropy presents a sudden increase at the accumulation point or transition to chaos $\mu = \mu_\infty$. After this sudden change in entropy, the phase corresponding to chaotic behavior yields larger values for the entropy, which is consistent.

Considering that the control parameter value plays the role of the temperature, we can think of an associated generalized susceptibility

$$\chi = \mu \left(\frac{\partial S}{\partial \mu} \right), \tag{4.29}$$

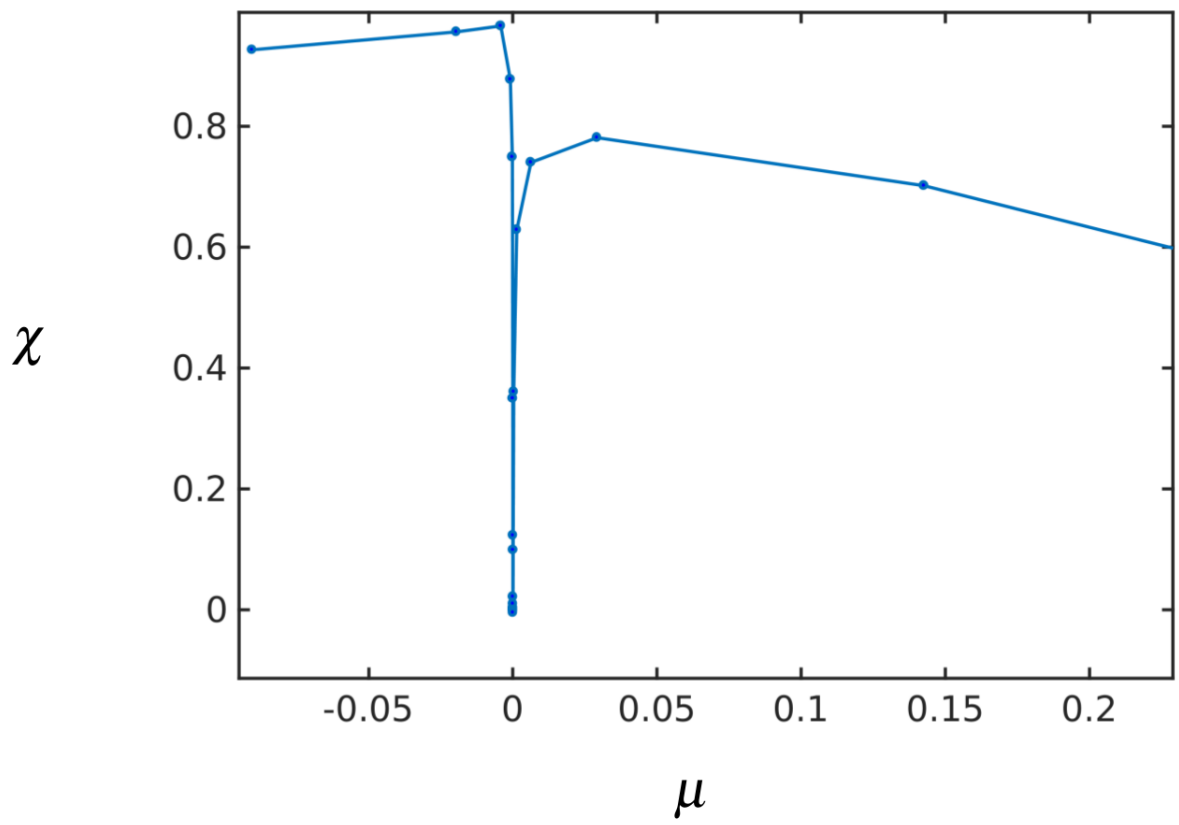

Figure 4.4: Susceptibility calculated according to $\chi = \mu \left(\frac{\partial S}{\partial \mu} \right)$.

Once the entropy is obtained, the whole thermodynamic framework can be constructed and proper connections with our formalism of the Frobenius-Perron densities can be adequately established. This will enable us to elucidate the connection between the microscopic dynamics of individual trajectories of the map and the macroscopic thermodynamic quantities we just found for the whole problem of the dual dynamical scenarios, both the routes out and into chaos. Which is more relevant here in our point of view, is that even when the densities are not absolutely continuous with respect to the Lebesgue measure, the Shannon entropy still gives results that are more or less sensible.

Chapter 5

Sums of positions and their distributions at the onset of chaos

Here we provide a thorough rationalization, backed by ample evidence, of the properties of sums of consecutive positions and their distributions for ensembles of trajectories associated with the sequence of chaotic 2^n-band attractors of the logistic map. We add to previous understanding [25, 31, 32] on the distributions of sums of positions at the period-doubling accumulation point for trajectories initiated within the attractor or with an ensemble of them uniformly-distributed across the entire phase space (the domain of the map). In the former case [31, 32] the support of the stationary distribution is the multifractal set that makes up the Feigenbaum attractor and its amplitude follows its multifractal nature. For the latter case [25] we demonstrated that the stationary distribution possesses an infinite-level hierarchical structure that originates from the properties of the repellor set and its preimages. We have also established [31, 32] that the entire problem $\lambda \geq 0$ can be couched in the language of the renormalization group RG formalism in a way that makes clear the identification of the existing stationary distributions and the manner in which they are reached. The RG transformation consists of position summation (and rescaling); there is only one relevant variable, the control parameter distance to the transition to chaos $\Delta\mu$. There are two fixed-point distributions, the trivial continuum-space gaussian distribution and the nontrivial multiscale distribution reached only when $\Delta\mu = 0$. The RG transformation modifies behavior similar to that of the nontrivial fixed point into that resembling the trivial fixed point through a well-defined crossover phenomenon. We show here that it is at this crossover region that the q-gaussian-like distributions are observed in Refs. [33–37]

The stationary distributions of sums of positions of trajectories generated by the logistic map have been found to follow a basic renormalization group (RG) structure: a nontrivial fixed-point multi-scale distribution at the period-doubling onset of chaos and a Gaussian trivial fixed-point distribution for all chaotic attractors. Here we describe in detail the crossover distributions that can be generated at chaotic band-splitting points that mediate between the aforementioned fixed-point distributions. Self-affinity in the chaotic region imprints scaling features to the crossover distributions along the sequence of band splitting points. The trajectories that give rise to these distributions are governed first by the sequential formation of phase-space gaps when, initially uniformly-distributed, sets of trajectories evolve towards the chaotic band attractors. Subsequently, the summation of positions of trajectories already within the chaotic bands closes those gaps. The possible shapes of the resultant distributions depend crucially on the disposal of sets of early positions in the sums and the stoppage of the number of terms retained in them.

Introduction

A few years ago a possible generalization of the central limit theorem (CLT) was put forward, as suitable for strongly correlated variables and that would have as its stationary distribution the so-called q-gaussian function [38]. Subsequently, it was surmised that a fitting model system for the observation of this generalization would be the period-doubling accumulation point of the logistic map [33]. This development led to increased interest and discussion [24, 26, 27, 31, 32, 34–37, 39, 40] about whether sums of correlated deterministic variables at vanishing, or near vanishing, Lyapunov exponent λ give rise to a general type of non-gaussian stationary distribution.

As it turned out [34], [36], [37], the distributions resembling q-gaussians at the period-doubling accumulation point require, unusual, specific procedures to be obtained. The first one is to work with a small but positive Lyapunov exponent $\lambda \gtrsim 0$. The second is to discard an initial tract of consecutive positions in the ensemble dynamics, the disposal of a 'transient', before evaluating the sum of the remaining positions. And the third is to stop the summation at a finite number of terms. When the transient set of terms is not discarded the resulting distribution would show an irregular, jagged, serrated, shape, whereas if the summation continues towards a larger and larger total number of terms the distribution approaches a gaussian shape. The q-gaussian-like distributions were observed along a sequence of values of the map control parameter μ that in latter studies [37] were identified as those approximately obeying the Huberman-Rudnick scaling law [41], the power law that relates distance in control parameter space to Feigenbaum's universal constant δ, or, equivalently, the number 2^n, $n = 0, 1, 2, \ldots$, of bands of the chaotic attractors.

In the following Section 2 we set up the elements of our analysis: The chaotic band splitting cascade of the logistic map [42, 43], along which we study trajectories at the control parameter points where bands split, also called Misiurewicz (M_n) points [44]. We focus on scaling properties for the sequence of M_n points. There we explain the dynamics undergone by an ensemble of uniformly distributed initial positions that consists of consecutive gap formation until arrival at the M_n attractor, after which intraband chaotic motion drives the dynamics. In Section 3 we present summations of positions and their distributions at various M_n points for different choices of disposal of initial sets of positions and different total number of summation terms. We explain the structure of the sums and their distributions in terms of the dynamics described in Section 2. In particular we detail the case that leads to distributions that resemble a q-gaussian shape. In Section 4 we discuss our results at some length in terms of the associated RG transformation.

Dynamics at chaotic band splitting points

We consider the logistic map $f_\mu(x) = 1 - \mu x^2$, $-1 \leq x \leq 1$, $0 \leq \mu \leq 2$, for which the control parameter value for its main period-doubling cascade accumulation point is $\mu = \mu_\infty = 1.401155189092...$ When μ is shifted to values larger than μ_∞, $\Delta\mu \equiv \mu - \mu_\infty > 0$, the attractors are chaotic and consist of 2^n bands, $n = 0, 1, 2, ...$, where $2^n \sim \Delta\mu^{-\kappa}$, $\kappa = \ln 2 / \ln \delta$, and $\delta = 4.669201609102\ldots$ is the universal constant that measures both the rate of convergence of the values of $\mu = \mu_n$ to μ_∞ at period doubling or at band splitting points. See Fig. 1a. The Misiurewicz (M_n) points, are attractor merging crises, where multiple pieces of an attractor merge together at the position of an unstable periodic orbit [44]. The M_n points can be determined by evaluation of the trajectories with initial condition $x_0 = 0$ for different values of μ, as these orbits follow the edges of the chaotic bands until at $\mu = \mu_n$ the unstable orbit of period 2^n reaches the merging crises [44].

Trajectories initiated inside a 2^n-band attractor consist of an interband periodic motion of period 2^n and an intraband chaotic motion. Trajectories initiated outside a 2^n-band attractor exit progressively a family

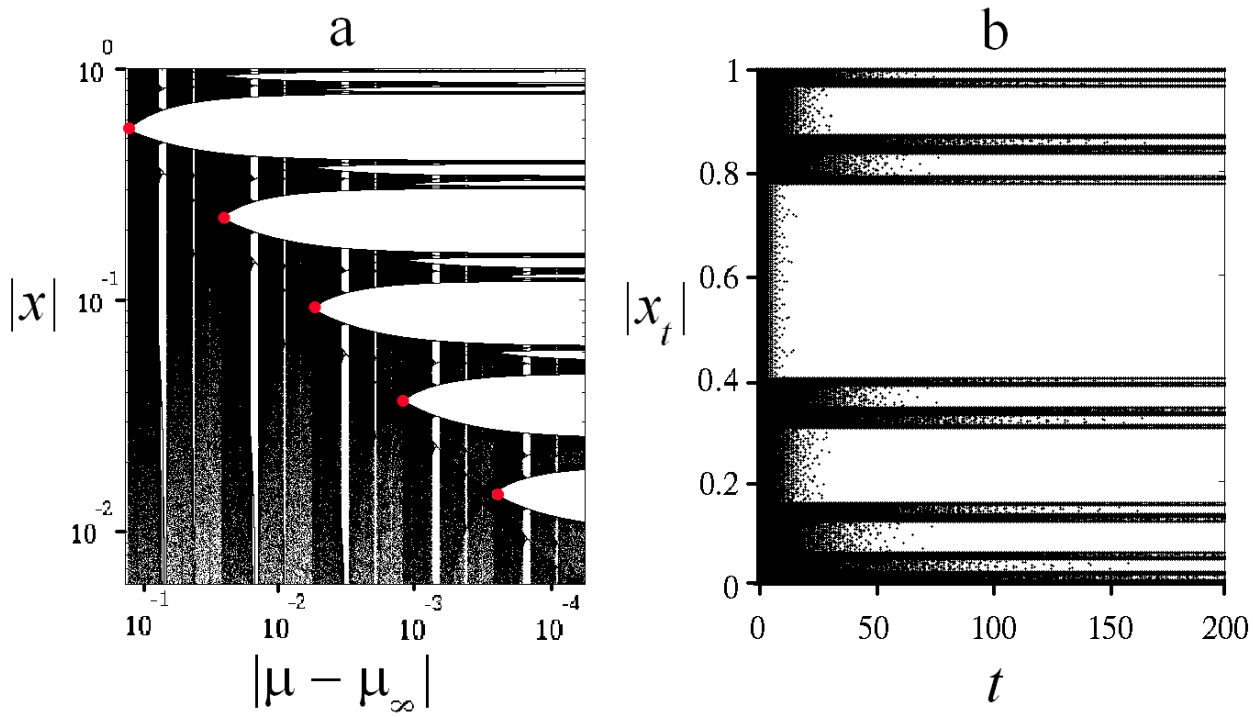

Figure 5.1: (a) Attractor bands (in black) and gaps between them (white horizontal regions) in logarithmic scales, $-\log(|\mu - \mu_\infty|)$ and $\log(|x|)$ in the horizontal and vertical axes, respectively. The band-splitting points M_n (circles) follow a straight line indicative of power law scaling. The vertical white strips are periodic attractor windows. (b) Sequential gap formation for M_5 by an ensemble of trajectories with initial conditions uniformly distributed along the map phase space. Black dots represent absolute values of trajectory positions $|x_t|$ at iteration time t. See text.

of sets of gaps formed in phase space between the 2^n bands. This family of sets of gaps starts with the largest gap formed around the first unstable orbit, or first repellor, of period 2^0, followed by two gaps containing the two positions of the second repellor of period 2^1, and so on. See Fig. 1b. The widths of the gaps diminish in a power law fashion as their numbers 2^k, $k = 0, 1, 2, ...$, for each set increase. We follow the dynamics towards the M_n, $n = 0, 1, 2, ...$, attractors by setting a uniformly-distributed ensemble of initial conditions across phase space, $-1 \leq x_0 \leq 1$, and record the normalized number of bins W_t, in a fine partition of this interval, that still contain trajectories at iteration time t. The results are shown in Fig. 2, where we observe an initial power law decay in W_t with logarithmic oscillations followed by a transition into a stay regime, a plateau with a fixed value of W_t, when (practically) all trajectories become contained and remain in the bands of the attractor.

The properties of W_t show discrete scale invariance associated with powers of 2 characteristic of unimodal maps. The number of logarithmic oscillations in the regime when trajectories flow towards the attractor coincides with the number of consecutive sets of gaps that need to be formed at the M_n points, whereas the final constant level of W_t coincides with the total number of bins that comprise the total width of the 2^n bands of the attractors. We notice that these properties when observed along the plateau entry points labeled t_n^* shown in Fig. 2 obey the Huberman-Rudnick scaling law since the times t_n^* are related to the 2^n bands of the M_n points and these in turn are given by $\Delta\mu_n \sim \delta^{-n}$.

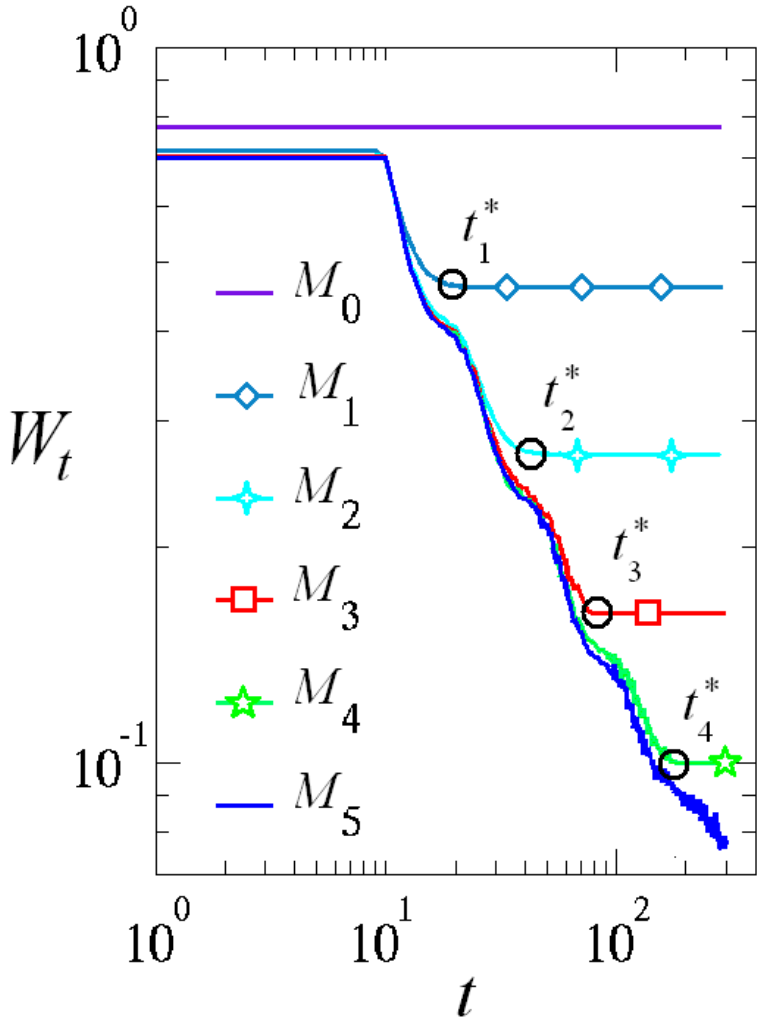

Figure 5.2: Distributions $P(Y;N_s,N_f;\mu_n)$ of zero mean sums $Y \equiv X - \langle X \rangle$, where X is given by Eq. (5.5). The sums were obtained from a uniform distribution of 10^6 initial conditions across $[-1,1]$ at M_5 when the attractor of 2^5 bands is about to split into 2^6 bands. A value of $N_s = 2^8$ is used in all panels. The values of N_f used are: (a) 2^5, (b) 2^9, (c) 2^{13} and (d) 2^{17}. See text.

Sums of positions and their distributions at band splitting points

Let us consider now the sum of consecutive positions x_t starting with an iteration time $t = N_s$ up to a final iteration time $t = N_f$ of a trajectory with initial condition x_0 and control parameter value μ fixed at a M_n point, $n = 0,1,2,...$, *i.e.*

$$X(x_0,N_s,N_f;\mu_n) \equiv \sum_{t=N_s}^{N_f} x_t. \tag{5.1}$$

We studied a collection of these sums for trajectories started from a uniform distribution of initial conditions in the entire interval $-1 \leq x_0 \leq 1$ with different values of n, N_s and N_f, and we also evaluated their corresponding histograms and finally their distributions by centering and normalization of the histograms. Clearly, stationary distributions require $N_f \to \infty$ and, unless there is some unusual circumstance, they are

not dependent on the value of N_s. We know [31], [32] that for all $\Delta\mu > 0$ the stationary distribution is gaussian and that in the limit $\Delta\mu = 0$ the stationary distribution is of an exceptional kind with intricate multiscale features [25, 35]. Here we explore other distributions that can be obtained when N_s and N_f are varied and identify the dynamical properties that give rise to them.

The observation of q-gaussian-like distributions in Refs. [34, 37], involved a large value of discarded terms N_s before sums similar to that in Eq. (5.5) were evaluated. Also, it was found necessary to limit the number of summands to a finite number N_f to prevent the distribution to approach a gaussian form. For example in Ref. [34] a fixed value of $N_s = 2^{12}$ was reported to be used for sums evaluated at attractors with a number of bands 2^n with n in the range 4 to 8. These sums were terminated, respectively, with values $N_f = 2^{n_f}$ with n_f in the range 9 to 17. In these studies the values of $\Delta\mu$ were not precisely fixed at band splitting points as we do here but the dynamical properties we describe are equivalent. We can understand the effect of the values of n, N_s and N_f used in terms of the dynamics of trajectories from the knowledge gained in the previous section. In references [34] and [37], the starting times $t = N_{s,n}$ in the sums in Eq. 5.5 satisfy the condition $t_n^* \ll N_{s,n}$. We can conclude with the assistance of Fig.2, that the terms discarded in those studies comprise the flow of trajectories towards the attractors plus a significant segment of dynamics within the chaotic bands, therefore all of the terms contained in the sums correspond to the dynamics within the chaotic bands.

As a representative example we show in Fig. 3 the distributions $P(Y;N_s,N_f;\mu_n)$ for the sums in Eq. (5.5), with $Y = X - \langle X\rangle$, and where $\langle X\rangle$ is the average of X over x_0. In this figure $n = 5$ and $N_s = 2^8$, and N_f takes the values $N_f = 2^5$, 2^9, 2^{13} and , 2^{17}, respectively, in panels (a), (b), (c) and (d). In (a) the sum comprises only one visit to each band and the structure of the distribution is the result of the one cycle intraband motion of the ensemble of trajectories. In (b) the sum contains already about $2^4 = 16$, band cycles, for which we obtain a distribution with q-gaussian-like shape but sharp drops at the edges. In (c) the q-gaussian-like shape is disappearing after 256 band cycles, while in (d), when there are 4096 band cycles, we observe already the stationary gaussian form. The same distribution progression pattern shown in Fig. 3 is observed at other M_n points. Furthermore, the sums and their distributions for any value of n can be reproduced by rescaling consistent with Huberman-Rudnick law. This is illustrated in Fig. 4 where we show in panels (a), (b) and (c) the resemblance of the centered sums Y for the band merging points M_3, M_4 and M_5, respectively. In panel (d) we show the distributions P for these sums without rescaling of the horizontal axis Y.

We have shown that there is an ample variety of distributions $P(Y;N_s,N_f;\mu_n)$ associated with the family of sums of iterated positions, as in Eq. (5.5), obtained from an ensemble of trajectories started from a uniform distribution of initial conditions in the interval $-1 \le x_0 \le 1$. The shapes of these distribution vary with N_s and N_f but there is scaling property with respect to n. All the types of distributions obtained can be understood from the knowledge of the dynamics that these trajectories follow, both when flowing towards the chaotic band attractors and when already within these attractors. There exists throughout the family of chaotic band attractors with $\lambda > 0$ an underlying scaling property, displayed, e.g., by the self-affine structure in Fig. 1a. This scaling property is present all over, here highlighted by: i) The sequential formation of gaps shown in Fig. 1b. ii) The number of bins W_t still containing trajectories at iteration time t, shown in Fig. **??**, both for its initial decay with logarithmic oscillations and the final constant regime. And iii) the different classes of sums and their distributions obtained for a given value of n are reproduced for other values of n under appropriate rescaling, as shown in Fig. 5.3. For adeptness and precision purposes we chose here to study the family of Misiurewicz points M_n but similar, equivalent, results are obtained for chaotic attractors between these points.

The discussion about the types of distributions $P(Y;N_s,N_f;\mu_{M_n})$ is assisted by recalling [31, 32] the RG framework associated with summation of positions. Positions x_t for trajectories within chaotic-band at-

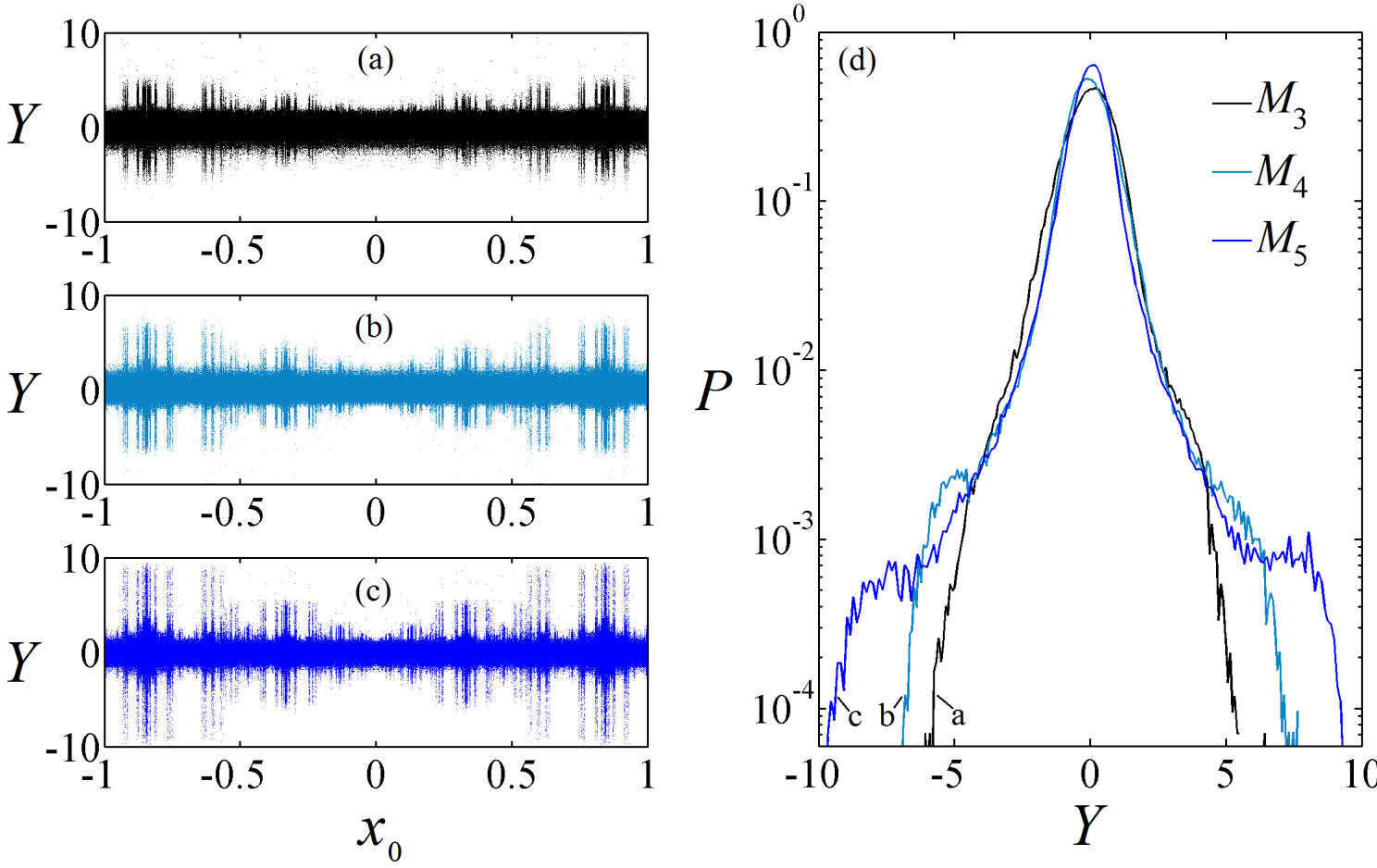

Figure 5.3: Rescaled sums and their distributions obtained from a uniform distribution of $3*10^6$ initial conditions across $[-1,1]$ at the band-splitting points M_n, $n=3,4,5$. The values of N_s and N_f used are, respectively $N_s=2^6,2^7,2^8$, and $N_f=2^{12},2^{13},2^{14}$.

tractors can be decomposed as $x_t = \overline{x}_t + \delta x_t$, where $\overline{x}_t$ is chosen to be (for example) fixed at the center of the band visited at time t and δx_t is the distance of x_t from $\overline{x}_t$. When the number of bands 2^n is large all the values of δx_t are small. The sum in Eq. (5.5) can be written as

$$X \equiv \overline{X} + \delta X,\ \overline{X} = \sum_{t=N_s}^{N_f} \overline{x}_t,\ \delta X = \sum_{t=N_s}^{N_f} \delta x_t, \tag{5.2}$$

where $\overline{X}$ captures the interband periodic (and therefore correlated) motion and δX consists of the intraband chaotic (and therefore random) motion. As discussed in Refs. [31,32] the action of the RG transformation, summation, is driven by δx_t and results in gradual widening of all the chaotic bands, such that eventually for a sufficiently large number of summands all of them merge into a single band. When $0 \leq N_{s,n} \lesssim t_n^*$ gap formation competes with band widening, while when $t^* \lesssim N_{s,n}$ band widening develops unimpeded. When $0 \leq N_{s,n} \lesssim t_n^*$ the combined processes of the dynamical evolution of the ensemble of trajectories and the repeated RG transformation is dominated initially by gap formation but it is always followed by gap merging. Initially, the distributions for these sums resemble the jagged multiscale shape of the stationary distribution for the nontrivial fixed point at $\Delta\mu = 0$ but they necessarily evolve towards the gaussian distribution of the trivial fixed point present for all $\Delta\mu > 0$ [31, 32]. When $t_n^* \ll N_{s,n}$, as in Refs. [33,34,36], [37], the trajectory positions considered in the sums are all contained within the attractor bands and from the first term $t = N_{s,n}$ the gaps begin to close due to the action of δx_t that is akin to an independent random variable. As we have shown in Fig. 3, when the number of summands grow the shape of the distribution evolves by first eliminating the initial serrated features, then developing a symmetrical shape that shows possible long tails but that end in a sharp drop (the claimed q-gaussian type), and finally the approach to the gaussian stationary distribution. All of the above can be observed for each 2^n-band chaotic attractor, basically from $n \geq 1$, and when a self-affine family of these attractors is chosen, like the Misiurewicz points M_n the sums and their distributions can be rescaled such that they just about match for all n, as shown in Fig. 5.3, where the sums where started at $N_{s,n} \simeq t_n^*$.
Concisely, the elimination of a large enough set of early positions in the sums for a given n, such that the location of its first term N_s is located inside the plateau of W_t in Fig. 2, ensures that the sums capture only the dynamics within the 2^n-band attractor. Therefore the shape of the distributions are dominated by the uncorrelated chaotic contributions δx_t, that as t increases evolves towards the final gaussian shape. A nongaussian distribution can only be obtained if there is a finite number of summands N_f. Self-affinity in the chaotic-band family of attractors, provides scaling properties to the distributions of sums of positions that are described by an appropriate use of the Huberman-Rudnick power-law expression.

Statistical aspects of the sums

In this section we * the study presented in the previous sections, thus considering the same scheme used in [28]. This study represents an opportunity for a closer analysis of the transformation of the distributions that initially possess multifractal characteristics that evolve toward the gaussian limit distribution. The larger the number 2^n of attractor bands, the finer is the approximation achieved to the multifractal structure of the distribution corresponding to the accumulation point before falling into the gaussian basin.
As a counterpart to our previous study of the stationary distribution formed by sums of positions at the Feigenbaum point via the period-doubling cascade in the logistic map [25], we determine the family of related distributions for the accompanying cascade of chaotic band-splitting points in the same system. By

*This section corresponds to the article [29].

doing this we rationalize how the interplay of regular and chaotic dynamics gives rise to either multiscale or gaussian limit distributions. As demonstrated before [31], sums of trajectory positions associated with the chaotic-band attractors of the logistic map lead only to a gaussian limit distribution, but, as we show here, the features of the stationary multiscale distribution at the Feigenbaum point can be observed in the distributions obtained from finite sums with sufficiently small number of terms. The multiscale features are acquired from the repellor preimage structure that dominates the dynamics toward the chaotic attractors. When the number of chaotic bands increases this hierarchical structure with multiscale and discrete scale-invariant properties develops. Also, we suggest that the occurrence of truncated q-gaussian-shaped distributions for specially prescribed sums are t-Student distributions premonitory of the gaussian limit distribution.

Here we consider again the logistic map. When the control parameter μ is changed toward values greater than μ_∞, this is $\Delta\mu = \mu - \mu_\infty > 0$, the corresponding attractors are mainly chaotic (except for the periodic windows) and consist of 2^n bands $n = 0,1,2,3,\ldots$, following the scaling law $2^n \sim \Delta\mu^{-\kappa}$, $\kappa = \ln 2/\ln\delta$. Among these chaotic attractors, we are only interested in the subsequence corresponding to the Misiurewicz points, that are regarded as dynamical crises [44]. In Fig. 5.4(a) we show (marked by different symbols) several M_n points that appear aligned due to the scales we used. The family of lines of equal slope along which the points M_n fall, reveal the scaling according to a power law associated to these positions. In Fig. 5.4(b) we show a corroboration of the occurrence of the gaussian limit distribution for the sums generated at the attractor for Ulam's map, which is composed by a single, fully chaotic region that covers the whole interval $x \in [-1,1]$ for $\mu = 2$, while in Fig. 5.4(c) we show the multifractal limit distribution corresponding to the Feigenbaum point at μ_∞.

In this section we show some statistical aspects regarding the sums originated by ensembles of positions and their corresponding distributions at Misiurewicz points. In particular, we are interested on the role that is played by the Student's-t distribution, or simply t distribution, for explaining the distributions associated to these sums. In one hand, we find that the distributions obtained from sums with a finite number of terms, when properly adjusted, this finite sum reproduces the asymmetric form with exponential tails of the limit distribution corresponding to μ_∞, and this gradually displays more of the characteristics of the underlying multifractal as the order n of the Misiurewcz point M_n increases. In the other hand, as the number N of terms in the sum increases, the distribution shows a rather symmetric form for each value n and eventually approaches the gaussian limit distribution as $N \to \infty$, just as it is expected for all the chaotic attractors. Finally and as the center of this work, we discuss the occurrence of the so-called q-gaussian distributions for a very special kind of sums in, or around the points M_n [28, 33, 34, 36, 37] in terms of the distributions that are standard in literature of probability and statistics [45]. These standard and well-known distributions are the result of a finite and rather poor sampling extracted from a population with a normal distribution, as it is the case of the aforementioned t distribution.

The stationary distributions of sums of consecutive positions of trajectories generated by the logistic map have been found to follow a basic renormalization group (RG) structure: a nontrivial fixed-point multiscale distribution at the period-doubling onset of chaos (Feigenbaum point) and a gaussian trivial fixed-point distribution for all chaotic attractors [31, 32]. At the Feigenbaum point the limit distribution of sums of positions, generated by an ensemble of initial conditions uniformly distributed in the full phase space, possesses an infinite-level hierarchical structure that originates from the properties of the repellor set and its preimages [25]. This ladder organization was elucidated [31] through consideration of the family of periodic attractors, conveniently, the super-stable attractors called supercycles [42], along the period-doubling cascade. Here we complement this study by considering instead the cascade of chaotic band-splitting attractors, or Misiurewicz $(M_n, n = 0,1,2,\ldots)$ points [28]. This gives us the opportunity of analyzing the

transformation of the developing multiscale distributions into the gaussian limit distribution. The larger the number 2^n of bands in the attractor the finer the approximation attained to the multiscale structure of the non-trivial fixed-point limit distribution before it undergoes a crossover to the gaussian distribution.

We consider the logistic map $f_\mu(x) = 1 - \mu x^2$, $-1 \leq x \leq 1$, $0 \leq \mu \leq 2$, for which the control parameter value for its main period-doubling cascade accumulation point is $\mu = \mu_\infty = 1.401155189092\ldots$ [**?**]. When μ is shifted to values larger than μ_∞, $\Delta\mu \equiv \mu - \mu_\infty > 0$, the attractors are (mostly) chaotic and consist of 2^n bands, $n = 0, 1, 2, ...$, where $2^n \sim \Delta\mu^{-\kappa}$, $\kappa = \ln 2 / \ln \delta$, and $\delta = 4.669201609102\ldots$ is the universal constant that measures both the rate of convergence of the values of $\mu = \mu_n$ to μ_∞ at period doubling or at band splitting points [42]. The latter points are attractor merging crises, where multiple pieces of an attractor merge together at the position of an unstable periodic orbit [44]. The M_n points can be determined by evaluation of the trajectories with initial condition $x_0 = 0$ for different values of μ, as these orbits follow the edges of the chaotic bands until at $\mu = \mu_n$ the unstable orbit of period 2^n reaches the merging crises [44]. In Fig. 6.1a we show (with different symbols) several M_n points that appear aligned because of the logarithmic scales employed. The family of lines of equal slope along which the M_n points fall reveal the power-law scaling associated with their locations. In Fig. 6.1b we show a corroboration for the gaussian limit distribution for sums generated at the one-band fully-chaotic attractor at $\mu = 2$, whereas in Fig. 6.1c we show the multiscale limit distribution for the Feigenbaum point at μ_∞.
Here we present results for ensembles of sums of positions and their distributions at the attractors where bands split. On the one hand, we find that distributions obtained from sums with an adequately finite number of terms resemble the asymmetric exponential-tailed shape of the limit distribution at μ_∞, and display gradually more of its multiscale features as the order n of the band-splitting point M_n increases. On the other hand, as the number of summands N increases the distribution for each value of n develops a symmetrical shape and eventually approaches the gaussian limit distribution for $N \to \infty$, as anticipated for all chaotic attractors. We discuss the occurrence of so-called q-gaussian distributions for special sums of positions at, or around, the M_n points [28], [46], [33] in terms of distributions for finite-size data sets drawn from gaussian variables such as it is the case of the t-Student distribution.

Sums of positions and their distributions for band-splitting attractors

We consider the sum of consecutive positions x_t up to a final iteration time N of a trajectory with initial condition x_0 and control parameter value μ, *i.e.*

$$X(x_0, N; \mu) \equiv \sum_{t=0}^{N} x_t \tag{5.3}$$

for $x_0 \in [-1, 1]$, as well as the centered, rescaled, sum

$$Y \equiv \frac{X - \langle X \rangle}{\sigma}, \tag{5.4}$$

where $\langle X \rangle$ is the average value for the sums over the ensemble of $\mathscr{M}$ initial conditions, and σ is the standard deviation of this ensemble. The use of Y instead of X facilitates the comparison between sums with different values of μ_n. We denote by H the histogram corresponding to the sum Y. H can be normalized or not, in which case it will be indicated.
The four panels in Fig. 6.7 show the results for $X(x_0, N; \mu)$ for all possible initial conditions $-1 \leq x_0 \leq 1$ when the control parameter takes the values for the first four Misiurewicz points, $M_n, n = 0, 1, 2, 3$. The

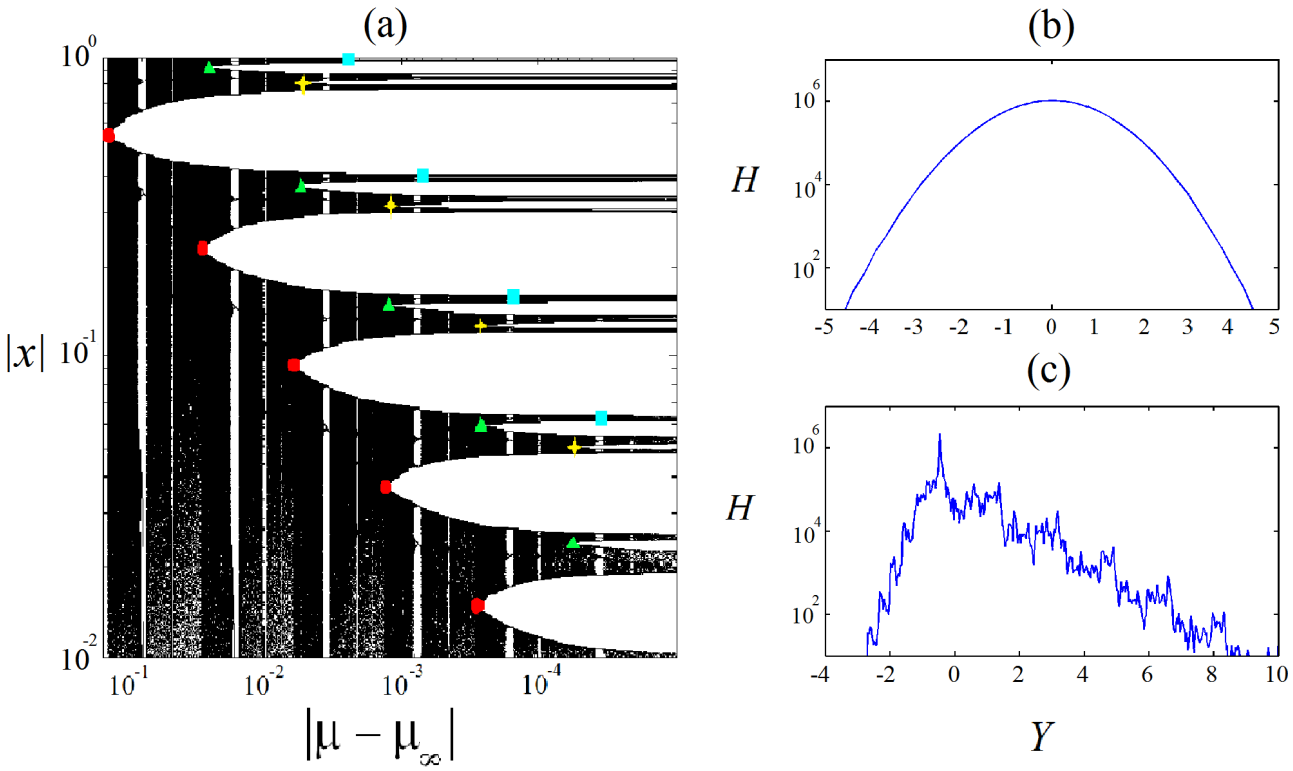

Figure 5.4: (a) Attractor bands (in black) and gaps between them (white horizontal regions) in logarithmic scales, $-\log(\mu - \mu_\infty)$ and $\log(|x|)$, in the horizontal and vertical axes, respectively. The band-splitting points M_n (circle, triangle, diamond and square symbols) follow straight lines indicative of power-law scaling. The vertical white strips are periodic attractor windows. (b) Histogram H of sums of trajectories when $\mu = 2$ approaches the shape of the gaussian limit distribution. (c) Histogram of sums of trajectories at $\mu = \mu_\infty$ approximates the shape of the multiscale limit distribution.

plots are all symmetrical with respect to $x_0 = 0$ and exhibit as a main feature two matching peaks and a central valley. For M_0 the two peaks and the valley are nearly concealed by other symmetrically-located peaks that form the fluctuating background generated by the large chaotic band that forms the attractor. But as the number of bands that form the attractor increases (and their widths decrease) for the subsequent M_1, M_2 and M_3 points the twin large peaks and other, finer, features become increasingly clear. This is the result of weaker intraband chaotic motion fluctuations as the interband regular dynamics progressively dominates.

The panels in Fig. 6.7 can be compared with those in Fig. 2 in [25] where the corresponding sums for the first supercycle attractors are shown. The same twin peaks separated by a central valley and progressively finer motifs of alternating signs appear in the sums of positions at the supercycle attractors [25], only there the absence of chaotic motion does not mask these details. In [25] it was demonstrated that these features in the sums arise from the dynamics towards the attractors. Namely, the two large peaks arise from the trajectories still close to the main repellor or its first preimage. Whereas the finer peaks of alternating signs are due to trajectory positions near subsequent repellors or their infinite families of preimages. See [25] for details. Here we observe, as shown in Fig. 6.7 that for the Misiurewicz points the same developments take place and that as the order n of M_n increases their effect on the sums becomes increasingly clear.

We look now at the distributions associated with the sets of sums $X(x_0, N; \mu)$ shown previously. The four panels in Fig. 5.6 present in semi-logarithmic scales the results for the (normalized) histograms that correspond to the sums in the panels for the first four Misiurewicz points, $M_n, n = 0, 1, 2, 3$ in Fig. 6.7. In the case of M_0 one obtains an almost round shape with some uneven, pointy, features at the right hand side. In the inset we show the attainment of a gaussian form when the number of summands is increased. The histogram for the next point M_1 already shows a basic tent shape formed by a sharp rise followed by a gentler decline. The following case M_2 displays serrated features over the tent shape that appear even more pronounced in the last case for M_3. Thus, as n increases we observe the development of the asymmetrical double-exponential global shape, with superimposed motifs of ever-decreasing finer detail, of the stationary distribution for μ_∞ shown in Fig. 6.1c.

Truncated q-gaussian (t-Student) crossover distributions at band-splitting attractors

Special sums of positions of ensembles of trajectories within the chaotic band attractors of the logistic map generate distributions that are well reproduced by truncated q-gaussian shapes [46], [33]. These sums are generated by first discarding an opening set of terms N_s such that the ensemble of trajectories initiated as a uniform distribution within $[-1, 1]$ is already located within the multiple-band attractor [28]. Secondly, the sums are stopped at a total number of terms N_f such that their distribution still displays large non-exponential, but truncated, tails. That is, these kind of sums are of the form

$$X(x_0, N_s, N_f; \mu) \equiv \sum_{t=N_s}^{N_s+N_f} x_t. \tag{5.5}$$

.

In Fig. 5.7 where we show in panels (a), (b) and (c) the centered sums $Y \equiv (X - \langle X \rangle)/\sigma$ for the Misiurewicz points M_3, M_4 and M_5, when the attractors are about to split into 16, 32 and 64 chaotic bands, respectively. In panel (d) we show the distributions P for these sums without rescaling of the horizontal axis Y. This kind of distributions have been fitted by q-gaussians [46], [33].

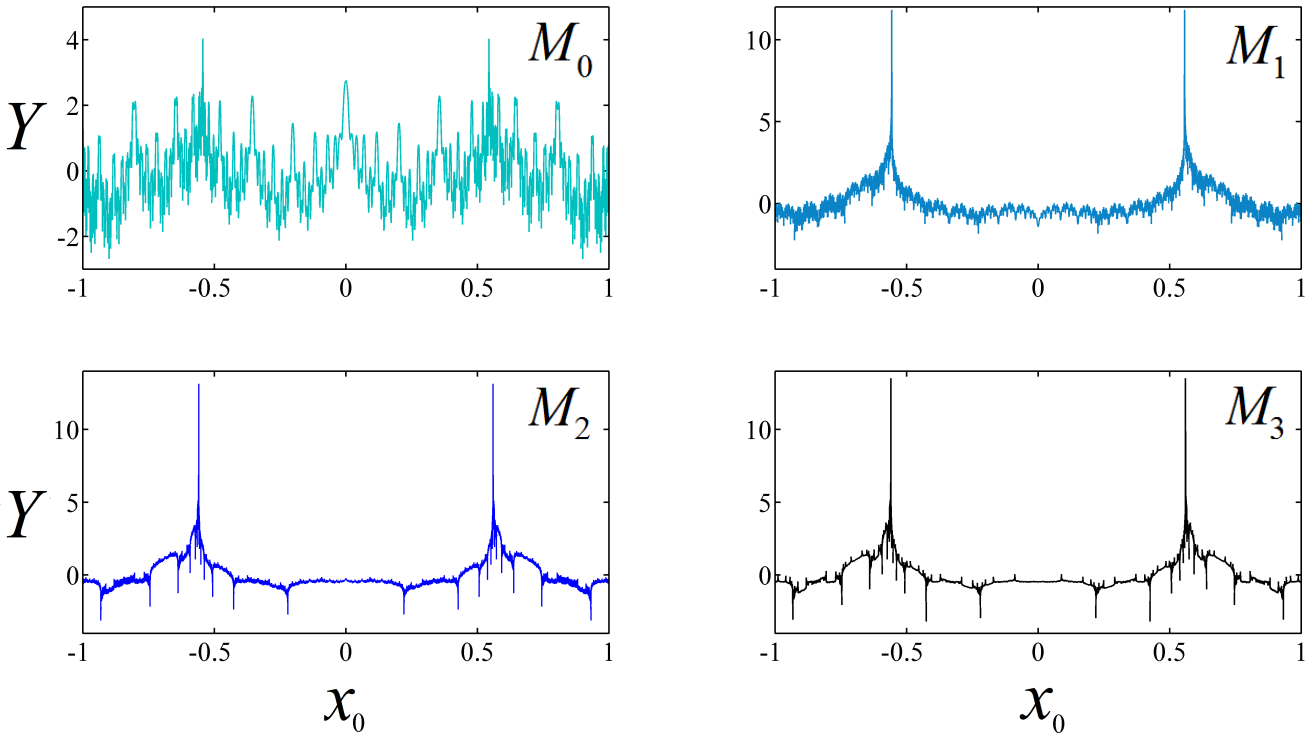

Figure 5.5: Sums $Y(x_0, N; \mu)$ as a function of the initial condition x_0. These correspond, as indicated in each frame, to the first four Misiurewicz points, M_0, M_1, M_2 and M_3, when the attractors are about to split into 2, 4, 8 and 16 chaotic bands, respectively. The number of terms in the sums for M_0, M_1, M_2 and M_3 are $N = 2^4, 2^5, 2^6, 2^7$, respectively. See text for description.

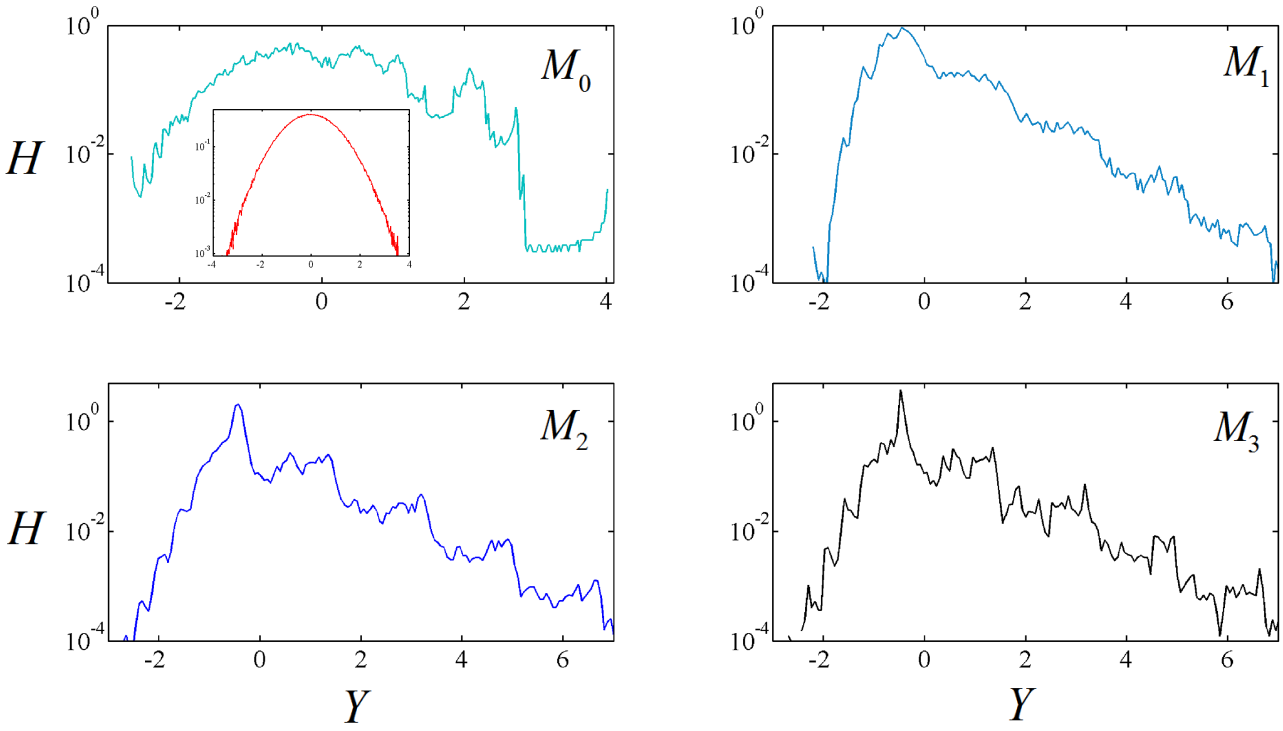

Figure 5.6: Normalized histograms H, obtained from the sums in Fig. 6.7. As indicated, these correspond to the first four Misiurewicz points, $M_n, n = 0,1,2,3$. In the inset for M_0 the sum consists of $O(2^{10})$ terms. See text for description

The Student's distribution or t-distribution is defined through the random variable

$$\vartheta = \frac{W\sqrt{n}}{\sqrt{Z}}, \tag{5.6}$$

where n is the sample size, the random variable X follows a gaussian distribution and Z is a random variable $Z = Z_1^2 + Z_2^2 + Z_3^2 + \ldots + Z_n^2$ following a χ^2-distribution. The sum in Eq. (5.5) when it is centered and rescaled as in Eq. (5.4), can be viewed as a random variable similar to that in Eq. (5.6) by including the crucial and delicate, but rather well-justified, assumption that the sums of positions follow a gaussian distribution. This is possible provided that the correlation function for the positions x_t goes to zero as the number of iterations N goes to infinity in a chaotic regime, as it is certainly fulfilled by the collection of Misiurewicz points we have used [43]. Under this assumption, the quantity in the numerator $\tilde{X} \equiv X - \langle X \rangle$ will (asymptotically) follow a gaussian distribution, and, considering the fact that the standard deviation in Eq. (5.4) is $\sigma = (1/\mathscr{M}\sum_i^{\mathscr{M}}(X_i - \langle X \rangle))^{1/2}$ we can write

$$Y = \frac{\tilde{X}\sqrt{\mathscr{M}}}{\sqrt{\tilde{Z}}}, \tag{5.7}$$

where we have considered $\tilde{Z}$ to be $\tilde{Z} = \sum_i^{\mathscr{M}} \tilde{X}_i$. The probability density function of the variable defined in Eq. (5.6) is

$$P(\vartheta) = \frac{\Gamma\left(\frac{n+1}{2}\right)}{(n\pi)^{1/2}\Gamma(\frac{n}{2})}\left(1 + \frac{\vartheta^2}{n}\right)^{-\frac{n+1}{2}}. \tag{5.8}$$

So we can expect, and then corroborate numerically, that our variable Y follows the same distribution, hence the sums of iterates Y can be regarded to follow a t-distribution. It is well known that the t-distribution arises when estimating the mean of finite data sets drawn from an infinite set that pertains to a gaussian distribution [45, 47]. The larger the sample the closer the t-distribution resembles the gaussian distribution and, in the limit $n \to \infty$ this is no longer an approximation and we recover a Gaussian, as we can check straightforwardly from Eq. (5.8).
It has been demonstrated [48] that this distribution optimizes the Tsallis entropy expression [46]. The expression for the t-distribution coincides (after a suitable change of variable) with that of the so-called q-gaussian distribution [48]

$$P(y) = \left(\frac{\beta(q-1)}{\pi}\right)^{\frac{1}{2}} \frac{\Gamma\left(\frac{1}{q-1}\right)}{\Gamma\left(\frac{1}{q-1} - \frac{1}{2}\right)}(1 + \beta(q-1)y^2)^{\frac{1}{1-q}}, \quad 1 < q < 3. \tag{5.9}$$

Therefore, the appearance of q-gaussian-like distributions for these families of sums are predictable as the chosen finite sets of data cannot still approximate the gaussian limit distribution. Interestingly, the t-Student (or q-gaussian) distribution maximizes an entropy expression that satisfies only three of the Khinchin axioms (with the exclusion of composability) [39] whereas the gaussian distribution maximizes the canonical entropy expression that satisfies all four Khinchin axioms.

Summary and discussion

We have probed the dynamical properties of chaotic attractors of the logistic map with the intention of learning about the distributions formed by sums of ensembles of positions of trajectories with uniformly-distributed initial conditions through the total phase space $[-1, 1]$. For suitability we chose members of

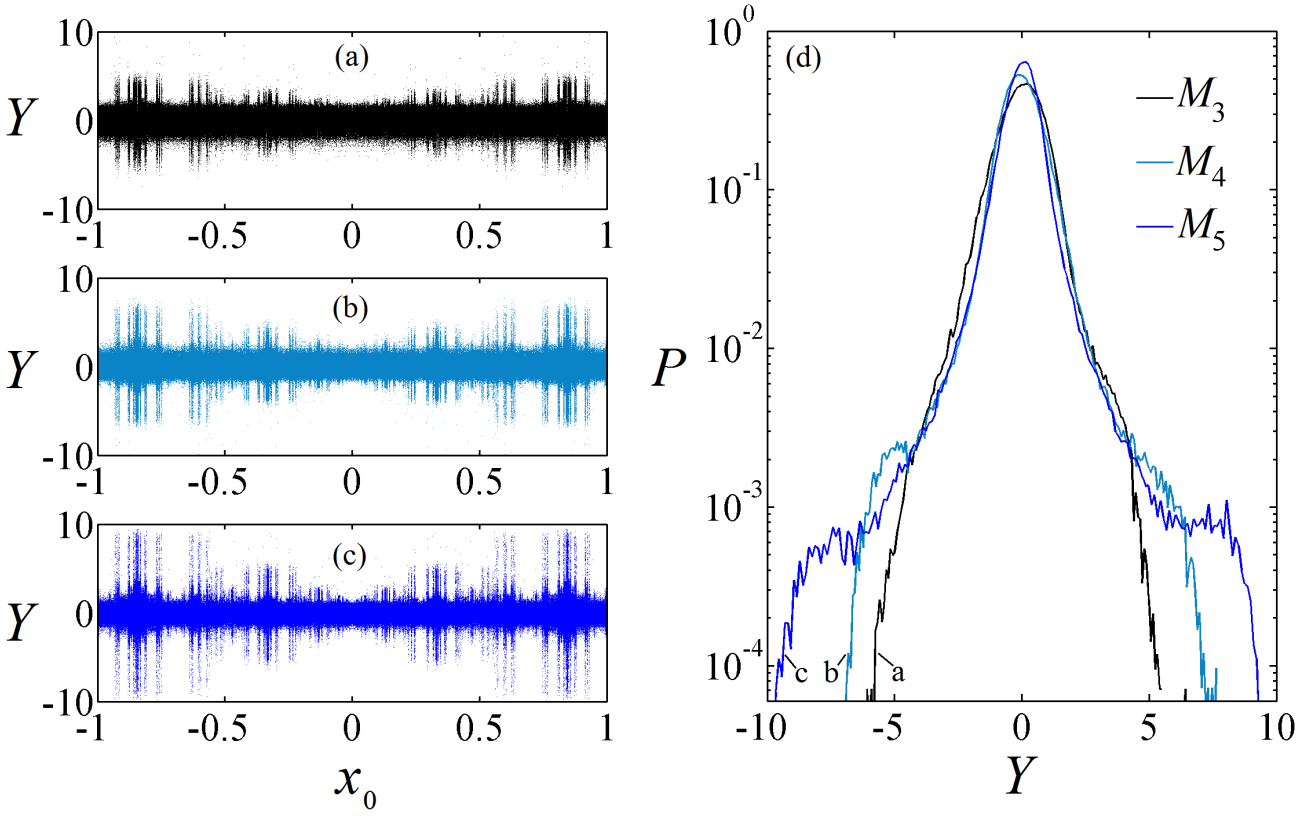

Figure 5.7: (Colour on-line.) Rescaled sums obtained from a uniform distribution of 10^6 initial conditions across $[-1,1]$ at the band-splitting points M_n, $n = 3,4,5$ with labels (a),(b),(c), respectively, and with their corresponding distributions (normalized histograms) P in (d). The values of N_s and N_f used are, respectively $N_s = 2^6, 2^7, 2^8$, and $N_f = 2^9, 2^{10}, 2^{11}$.

the family of attractors at which bands split. Our results are consistent with the existence of a single type of limit distribution (i.e. when the number of summands $N \to \infty$) for all chaotic attractors, this being the gaussian distribution. But we also observed, when the sums have a sufficiently small number of terms, the characteristic features of the multiscale, asymmetric, exponential-tailed, limit distribution that occurs for the special case of the accumulation point of the band-splitting attractors, the Feigenbaum point at μ_∞. The crossover that takes place from distributions displaying the multiscale form to the gaussian shape was also addressed. Sums obtained when all trajectories are placed within the chaotic bands and are built-up from finite sets of positions that evolve randomly are comparable to sets of variables extracted from a gaussian population as this is their limit distribution. Such procedure generates the t-Student distribution, equivalently a q-gaussian distribution, as previous studies detected.

Part III

Dimensional reduction in a model of evolutionary ecology.

Chapter 6

From high to low dimensions in a model of evolutionary ecology.

It is well known that low-dimensional nonlinear deterministic maps close to a tangent bifurcation exhibit intermittency and this circumstance has been exploited, *e.g.* by Procaccia and Schuster [49], to develop a general theory of $1/f$ spectra. This suggests it is interesting to study the extent to which the behavior of a high-dimensional stochastic system can be described by such tangent maps. The Tangled Nature (TaNa) Model of evolutionary ecology is an ideal candidate for such a study, a significant model as it is capable of reproducing a broad range of the phenomenology of macroevolution and ecosystems. The TaNa model exhibits strong intermittency reminiscent of Punctuated Equilibrium and, like the fossil record of mass extinction, the intermittency in the model is found to be non-stationary, a feature typical of many complex systems. We derive a mean-field version for the evolution of the likelihood function controlling the reproduction of species and find a local map close to tangency. This mean-field map, by our own local approximation, is able to describe qualitatively only one episode of the intermittent dynamics of the full TaNa model. To complement this result we construct a complete nonlinear dynamical system model consisting of successive tangent bifurcations that generates time evolution patterns resembling those of the full TaNa model in macroscopic scales. The switch from one tangent bifurcation to the next in the sequences produced in this model is stochastic in nature, based on criteria obtained from the local mean-field approximation, and capable of imitating the changing set of types of species and total population in the TaNa model. The model combines full deterministic dynamics with instantaneous parameter random jumps at stochastically drawn times. In spite of the limitations of our approach, that entails a drastic collapse of degrees of freedom, the description of a high-dimensional model system in terms of a low-dimensional one appears to be illuminating.

Intermittent dynamics and evolutionary ecology

Intermittent dynamics in the form of long periods of little change separated by relatively short time intervals of hectic activity is observed in many complex systems. Examples include snoring, mass extinctions, financial crashes and brain activity. Such systems contain large numbers of components and very often involve stochastic processes. It was more than 40 years ago suggested by Procaccia and Schuster that important aspects of such intermittent dynamics can be captured by a simple essentially deterministic equation. It is not in general straight forward to connect in detail the complex system to the mathematics considered by Procaccia and Schuster. We consider a multi-component model of evolutionary ecology and

derive how the single component equation of the type considered by Procaccia and Schuster is related to the parameters of the stochastic many component dynamics. The single component description enables us to describe aspects of the intermittent extinction dynamics that so far has eluded mathematical analysis. We also demonstrate that the single component mathematics is able to qualitatively mimic the evolution and extinction dynamics of consecutive ecologies generated by the full many component model. We think that our results expands the applicability of the analysis put forward by Procaccia and Schuster and thereby help connect the methodology developed for deterministic and typically low dimensional dynamics to the stochastic dynamics of complex systems.

High-dimensional complex systems, such as turbulence, relaxing glasses, biological evolution, the financial market or brain dynamics, exhibit intermittent dynamics [50, 51]. While intermittency in basic one-dimensional non-linear maps at the so-called tangent bifurcation [51] has received significant attention *e.g.* because of their universal aspects [52] and has been suggested as a universal mechanism for $1/f$ noise [53]. In fact the paradigmatic Pomeau-Manneville map [54] was derived to represent intermittency in weakly turbulent fluid dynamics. The relevance of such maps to high-dimensional stochastic systems depends on whether a robust macroscopic degree of freedom emerges, which is able to capture the dominant dynamics. A case in point is the Tangled Nature (TaNa) model [50] of evolutionary ecology, since it displays intermittent evolution at the macroscopic level while microscopically individuals reproduce, mutate and die at essentially constant rates [55, 56]. Numerical simulations of the model show that the total population $N(t)$ as a function of time t (in the scale of generations) consists of quasi-stable, steady, periods that alternate with interludes of hectic transitions, during which $N(t)$ exhibits large amplitude fluctuations [55, 56]. The populations of species behave accordingly, during the quasi-stable periods they predominantly retain their identity, but at the transitions some species vanish, others arise, while the rest survive [55, 56].

Here we study the incidence of intermittency, as displayed close to the tangent bifurcation in low-dimensional nonlinear maps, in the macroscopic behavior of the TaNa model. We make two intents. The first one is to approximate the evolution equations of the model, via determination of mean-field lowest-order local terms to obtain a map near tangency that reproduces the prototypical quasi-stable episode. The second is to model, phenomenologically, the sequences of consecutive quasi-stable and hectic periods via a nonlinear dynamical model that makes use of the families of tangent bifurcations that occur in one-dimensional quadratic maps. We arrive at the following general picture. The dynamics of the original TaNa model is fully stochastic and fluctuations are very important in steering its progress. The one-dimensional mean-field local map near tangency, we derive, is deterministic and has the limitation, without further development, that only one quasi-stable event can be generated at a time. But this map offers criteria for the duration of the quasi-stable episodes in terms of the TaNa model parameters. Based on these criteria we introduce a stochastic element in the construction of an otherwise deterministic nonlinear dynamical model. This model reproduces qualitatively the sequences of quasi-stable periods with varying types and numbers of species as in the TaNa model. We comment on the class of nonlinear dynamical systems with this kind of stochastic element. We reach the conclusion that in spite of the approximations incurred and assumptions made our study facilitates interesting insights that hint to a radical reduction of degrees of freedom under certain circumstances.

High-dimensional complex systems, such as turbulence, relaxing glasses, biological evolution, the financial market or brain dynamics, exhibit intermittent dynamics [50, 51]. While intermittency in basic one-dimensional non-linear maps at the so-called tangent bifurcation [51] has received significant attention *e.g.* because of their universal aspects [52] and has been suggested as a universal mechanism for $1/f$ noise [53]. In fact the paradigmatic Pomeau-Manneville map [54] was derived to represent intermittency in weakly turbulent fluid dynamics. The relevance of such maps to high-dimensional stochastic systems depends on whether a robust macroscopic degree of freedom emerges, which is able to capture the dominant dynamics.

A case in point is the Tangled Nature (TaNa) model [50] of evolutionary ecology, since it displays intermittent evolution at the macroscopic level while microscopically individuals reproduce, mutate and die at essentially constant rates [55,56]. Numerical simulations of the model show that the total population $N(t)$ as a function of time t (in the scale of generations) consists of quasi-stable, steady, periods that alternate with interludes of hectic transitions, during which $N(t)$ exhibits large amplitude fluctuations [55,56]. The populations of species behave accordingly, during the quasi-stable periods they predominantly retain their identity, but at the transitions some species vanish, others arise, while the rest survive [55,56].
Here we study the incidence of intermittency, as displayed close to the tangent bifurcation in low-dimensional nonlinear maps, in the macroscopic behavior of the TaNa model. We make two intents. The first one is to approximate the evolution equations of the model, via determination of mean-field lowest-order local terms to obtain a map near tangency that reproduces the prototypical quasi-stable episode. The second is to model, phenomenologically, the sequences of consecutive quasi-stable and hectic periods via a nonlinear dynamical model that makes use of the families of tangent bifurcations that occur in one-dimensional quadratic maps. We arrive at the following general picture. The dynamics of the original TaNa model is fully stochastic and fluctuations are very important in steering its progress. The one-dimensional mean-field local map near tangency, we derive, is deterministic and has the limitation, without further development, that only one quasi-stable event can be generated at a time. But this map offers criteria for the duration of the quasi-stable episodes in terms of the TaNa model parameters. Based on these criteria we introduce a stochastic element in the construction of an otherwise deterministic nonlinear dynamical model. This model reproduces qualitatively the sequences of quasi-stable periods with varying types and numbers of species as in the TaNa model. We comment on the class of nonlinear dynamical systems with this kind of stochastic element. We reach the conclusion that in spite of the approximations incurred and assumptions made our study facilitates interesting insights that hint to a radical reduction of degrees of freedom under certain circumstances.

The TaNa model

The Tangled Nature model is a model of evolutionary ecology, which studies the macro-dynamics emerging from the dynamics of individual organisms or agents, co-evolving together and subject to a web of mutual interactions. The model is an attempt to identify possible simple mechanisms behind the myriad of complicated interactions, feedback loops, contingencies, etc., as one moves from the short time reproductive dynamics at the level of individuals, to the long time systems level behaviour. The strategy is to keep the model sufficiently simple to enable analysis, and to pinpoint the details or assumptions in the model that are responsible for the specific behaviour at the systems level. One major concern of the model has been to understand how the smooth continuous pace of the reproductive dynamics at the level of individuals, can lead to intermittent or punctuated dynamics at the level of high taxonomic structures. The model was introduced in [55, 56] and since then, the model framework has been used by several authors see *e.g.* [57–61]. A summary of some of the models features and predictions can be found in [50].

Description of the model

The dynamical entities of the TaNa model consist of agents represented by a sequence of binary variables with fixed length L [62]. We denote by $n(\mathbf{S}^a,t)$ the number of agents of type $\mathbf{S}^a = (S_1^a, S_2^a, ..., S_L^a)$ (here $S_i^a \in \{-1,1\}$)at time t and the total population is $N(t) = \sum_{a=1}^{2^L} n(\mathbf{S}^a,t)$. A time step is defined as a succession of one annihilation and of one reproduction attempt. Annihilation consists of choosing an agent at random

with uniform probability and remove the agent with probability p_{kill}, taken to be constant in time and independent on the type. Reproduction: choose with uniform probability an agent, $\mathbf{S^a}$, at random and duplicate the agent (and remove the mother) with probability

$$p_{off}(\mathbf{S}^a,t) = \frac{\exp\left(H(\mathbf{S}^a,t)\right)}{1+\exp\left(H(\mathbf{S}^a,t)\right)}, \tag{6.1}$$

which depends on the occupancy distribution of all the types at time t through the weight function

$$H(\mathbf{S}^a,t) = \frac{k}{N(t)}\sum_b J(\mathbf{S}^a,\mathbf{S}^b)n(\mathbf{S}^b,t) - \mu N(t). \tag{6.2}$$

In Eq. (6.2), the first term couples the agent $\mathbf{S}^a$ to one of type $\mathbf{S}^b$ by introducing the interaction strength $\mathbf{J}(\mathbf{S}^a,\mathbf{S}^b)$, whose values are randomly distributed in the interval $[-1,+1]$. For simplification and to emphasize interactions we here assume: $\mathbf{J}(\mathbf{S}^a,\mathbf{S}^a) = 0$. The parameter k scales the interactions strength and μ can be thought of as the carrying capacity of the environment. An increase (decrease) in μ corresponds to harsher (more favourable) external conditions.
Mutations occur in the following way: For each of the two copies $\mathbf{S}^{a_1}$ and $\mathbf{S}^{a_2}$, a single mutation changes the sign of one of the genes: $S_i^{a_1} \to -S_i^{a_1}$, $S_i^{a_2} \to -S_i^{a_2}$ with probability p_{mut}. We define a generation to consist of $N(t)/p_{kill}$ time steps, *i.e.* the average time needed to kill all the individuals at time t. These microscopic rules generate intermittent macro dynamics [56] as shown in Fig. 6.1. The long quiescent epochs are called quasi Evolutionary Stable Strategies (qESS), since they do remind one of John Maynard Smith's notion of Evolutionary Stable Strategies introduced in his game theoretic description of evolution [63].
The weight function H will fluctuate about the value given by the stable dynamical fixed point condition $p_{off}(H) = p_{kill}$. This suggests that the mean field value of H may indeed evolve in an intermittent way that may be captured by a tangent map. We will therefore derive the mean field map for $\langle H\rangle$.

Mean field mapping derivation for H

To establish a map for the mean field approximation to the weight function H, we need to analyse each of the microscopic stochastic processes that can lead to a change in H. These are reproduction, with or without mutation and death. And we will make use of the fact that if a quantity, say X, undergoes the change to $X \mapsto X+\Delta$ with probability p and remains unchanged $X \mapsto X$ with probability $1-p$, then in the mean field approximation we have $\langle X\rangle \mapsto \langle X\rangle + p\Delta$. We use a short hand notation in which we label individuals and types as $i,j,k...$ and accordingly the interaction between two types i and j as J_{ij}.

Reproduction with no mutation. We need to estimate the average change to the likelihood function, H_i for type i given that an individual of type j_0 reproduces without mutating. The change in H_i is given by

$$\begin{aligned} H_i &\mapsto \frac{k}{N+1}\left[\sum_{j\neq j_0} J_{i,j}n_j + J_{i,j_0}(n_{j_0}+1)\right] - \mu(N+1) \\ &= \frac{k}{N+1}\left(\sum_j J_{i,j}n_j - \mu N\right) + \left(\frac{k}{N+1}J_{i,j_0} - \mu\right) \\ &= H_i + \Delta^i_{R,0m}(j_0) \end{aligned} \tag{6.3}$$

We replaced $N+1$ by N in the first term and introduced the change

$$\Delta^i_{R,0m}(j_0) = \frac{k}{N+1} J_{i,j_0} - \mu, \tag{6.4}$$

which will occur with probability

$$p^i_{R,0m}(j_0) = \frac{n_{j_0}}{N} p_{off}(j_0)(P^{(0)}_{mut})^2, \tag{6.5}$$

where $P^{(0)}_{mut} = (1-p_{mut})^L$ is the probability of no mutations occurring, and its counted twice, once for each offspring. Averaging over all possible types (of which there are $\Omega = 2^L$) we obtain

$$\begin{aligned} \bar{\Delta}_{R,0m} &= \langle \Delta^i_{R,0m}(j_0) \rangle = \frac{1}{\Omega} \sum_{j_0} \left(\frac{k}{N} J_{ij_0} - \mu \right) \frac{n_{j_0}}{N} p_{off}(j_0)(P^{(0)}_{mut})^{2L} \\ &\mapsto \left(\frac{k\bar{J}}{N} - \mu \right) \langle p_{off} \rangle_{ext} (1-p_{mut})^{2L}, \end{aligned} \tag{6.6}$$

where we have introduced $\bar{J}$, which denotes the strengths $J_{i,j}$ averaged over pairs of interacting extant types and similarly $\langle p_{off} \rangle_{ext}$ denotes the offspring probability average over extant types.

Reproduction with 1 mutation Next we consider the average change to the likelihood function, H_i for type i given that an individual of type j_0 reproduces with one copy mutating and ending in q_o and the other not mutating. The change in H_i is given by

$$\begin{aligned} H_i &\mapsto \frac{k}{N+1} \left[\sum_{j \neq q_0} J_{i,j} n_j + J_{i,q_0}(n_{q_0}+1) \right] - \mu(N+1) \\ &= \frac{k}{N+1} \left(\sum_j J_{i,j} n_j - \mu N \right) + \left(\frac{k}{N+1} J_{i,q_0} - \mu \right) \\ &= H_i + \Delta^i_{R,m}(q_0). \end{aligned} \tag{6.7}$$

Again we have replaced $N+1$ by N in the first term and introduced the change

$$\Delta^i_{R,m}(q_0) = \frac{k}{N+1} J_{i,q_0} - \mu, \tag{6.8}$$

which will occur with probability

$$p^i_{R,m}(j_0) = \frac{n_{j_0}}{N} p_{off}(j_0) p_{j_o \to q_o}, \tag{6.9}$$

where

$$p_{j_o \to q_o} = p^{d_{j_o q_o}}_{mut} (1-p_{mut})^{L - d_{j_o q_o}}, \tag{6.10}$$

and $d_{j_o q_o}$ is the hamming distance between the sequences j_o and q_o, This means that

$$\bar{\Delta}^i_{R,1m} = \sum_{j_o q_o} \left(\frac{k}{N+1} J_{i,q_o} - \mu \right) \frac{n_{j_o}}{N} p^{off}_j p^{d_{j_o q_o}}_{mut} (1-p_{mut})^{L - d_{j_o q_o}}. \tag{6.11}$$

By limiting our approximation to the nearest neighbours, and proceeding like in the previous case, we obtain

$$\bar{\Delta}_{R,1m} = L p^{(o)}_{mut} p^{(1)}_{mut} \left(\frac{k\tilde{J}}{N} - \mu \right) \langle p_{off} \rangle_{ext}, \tag{6.12}$$

where L is the number of first neighbours and $P^{(1)}_{mut} = p_{mut}(1-p_{mut})^{(L-1)}$ denotes the probability that exactly one L genes mutate. Notice the difference between $\bar{J}$ introduced in Eq. (6.6) and the averaged quantity $\tilde{J}$ introduced in this equation. The two differs by being averages over different sets of types. Here $\tilde{J}$ is averaged over interaction strengths J_{ij} connecting already occupied type and types hit by a new mutation, *i.e.* types located in the perimeter of the cluster of extant reproducing sites. In contrast $\bar{J}$ is the average of the interaction strength between extant types. We will expect that typically $\tilde{J} < \bar{J}$ because adaptation has favoured mutualistic interactions amongst the extant types. However, an accurate estimate of the two quantities from first principle is of course very difficult.

Reproduction with 2 mutations. Next we consider the average change to the likelihood function, H_i for type i given that an individual of type j_0 reproduces with both copies mutating and ending in q_o and q_1. The change in H_i is given by

$$\begin{aligned} H_i &\mapsto \frac{k}{N+1} \left[\sum_{j \neq q_0, q_1, j_o} J_{i,j} n_j + J_{i,q_0}(n_{q_0}+1) + J_{i,q_1}(n_{q_1}+1) + J_{i,q_1}(n_{q_1}-1) \right] - \mu(N+1) \\ &= \frac{k}{N+1} \left(\sum_j J_{i,j} n_j - \mu N \right) + \left(\frac{k}{N+1}(J_{i,q_0} + J_{i,q_1} - J_{i,j_o}) - \mu \right) \\ &= H_i + \Delta^i_{R,2m}(q_0), \end{aligned} \tag{6.13}$$

where we have consider the fact that the number of individuals of the parent decreases in case of 2 mutations. Again we have replaced $N+1$ by N in the first term and introduced the change

$$\Delta^i_{R,2m}(q_0) = \frac{k}{N+1}(J_{i,q_0} + J_{i,q_1} - J_{i,j_o}) - \mu, \tag{6.14}$$

which will occur with probability

$$p^i_{R,m}(j_0) = \frac{n_{j_0}}{N} p_{off}(j_0) p_{j_o \to q_o} p_{j_o \to q_1}. \tag{6.15}$$

And once again limiting our approximation to the nearest neighbour mutations we obtain

$$\bar{\Delta}_{R,2m} = L^2 (P^{(1)}_{mut})^2 \left(\frac{k\tilde{J}}{N} - \mu \right) \langle p_{off} \rangle_{ext}. \tag{6.16}$$

Notice the difference between $\bar{J}$ introduced in Eq. (6.6) and the averaged quantity $\tilde{J}$ introduced in this equation. The two differs by being averages over different sets of types. Here $\tilde{J}$ is averaged over interaction strengths J_{ij} connecting already occupied type and types hit by a new mutation, *i.e.* types located in the perimeter of the cluster of extant reproducing sites. In contrast $\bar{J}$ is the average of the interaction strength between extant types. We will expect that typically $\tilde{J} < \bar{J}$ because adaptation has favoured mutualistic interactions amongst the extant types. This is in fact verified by our simulations, see Fig. 6.3 below.

Killing event on site j_0 leads to

$$\begin{aligned} H_i &\mapsto \frac{k}{N-1}\left[\sum_{j\neq j_0} J_{i,j}n_j + J_{i,0_0}(n_{j_0}-1)\right] - \mu(N-1) \\ &= \frac{k}{N-1}\left(\sum_j J_{i,j}n_j - \mu N\right) - \left(\frac{k}{N}J_{i,j_0} - \mu\right) \\ &= H_i - \Delta^i_{R,0m}(j_0). \end{aligned} \tag{6.17}$$

This change occurs with probability $(n_{j_0}/N)p_{kill}$.
Combining this result with the weighted results in Eqs. (6.6), (6.12) and (6.16) we obtain the following map, which in mean field describes how $\langle H\rangle$ changes as an effect of the microscopic reproduction and killing events

$$\langle H\rangle \mapsto \langle H\rangle + A\langle p_{off}\rangle_{ext} - Bp_{kill}, \tag{6.18}$$

where the coefficients are given by

$$A = \left(\frac{k\bar{J}}{N} - \mu\right)(P^{(0)}_{mut})^2 + \left(\frac{k\tilde{J}}{N} - \mu\right)(P^{(0)}_{mut} + Lp^{(1)}_{mut})Lp^{(1)}_{mut} \tag{6.19}$$

$$B = \frac{k\bar{J}}{N} - \mu \tag{6.20}$$

We have derived a map for the evolution of $\langle H\rangle$. We now need to close the map, *i.e.* we need a way to express the H^i dependency of $\langle p_{off}\rangle_{ext}$ in terms of $\langle H\rangle$. We could assume

$$\langle p_{off}(H^i)\rangle_{ext} \mapsto p_{off}(\langle H\rangle_{ext}). \tag{6.21}$$

This procedure gives us the following map for x_n (which we use as shorthand for the iterates of $\langle H\rangle_{ext}$)

$$x_{n+1} = x_n + Ap_{off}(x_n) - Bp_{kill}. \tag{6.22}$$

The map has a fixed point a x^* given by $p_{off}(x^*) = Bp_{kill}/A$. The map is stable if $A < 0$ and $B < 0$. For $AB < 0$ the map is either attractive (repulsive) to the left of x^* and repulsive (attractive) to the right hand of x^*. For $A < 0$ and $B < 0$ x^* is repulsive in both directions. The conclusion is that the dramatic mean field approximation suggested in Eq. (6.21), which corresponds to the replacement $\langle H^n\rangle_{ext} \mapsto \langle H\rangle^n_{ext}$ for all $n \in \mathbb{N}$, wipes out the intermittency. To establish a mean field description of the intermittency we instead expand $p_{off}(H^i)$ in Eq. (6.18) to second order about x^* and replaces only $\langle H^2\rangle_{ext}$ by $\langle H\rangle^2_{ext}$. This leads to a tangent map and we study the intermittency of this map in the next section.

Analysis close to tangency

We expand $p_{off}(H)$ in Eq. (6.18) to second order about $H^* = \ln[p_{kill}/(1-p_{kill})]$,

$$p_{off}(H) = a_0 + a_1(H - H^*) + a_2(H - H^*)^2 \tag{6.23}$$

where

$$\begin{aligned} a_0 &= p_{kill}, \\ a_1 &= p'_{off}(H^*) = p_{kill}(1-p_{kill}), \\ a_2 &= \frac{1}{2}p''_{off}(H^*) = \frac{1}{2}a_1(1-2p_{kill}). \end{aligned}$$

We substitute Eq. (6.23) into Eq. (6.22) and obtain the following map for $\Delta = \langle H \rangle - H^*$

$$\Delta_{n+1} = b_0 + b_1 \Delta_n + b_2 \Delta_n^2 \equiv f(\Delta_n), \tag{6.24}$$

where

$$\begin{aligned} b_0 &= a_0(A-B), \\ b_1 &= 1 + a_1 A, \\ b_2 &= a_2 A. \end{aligned}$$

Let Δ_c be given by $f'(\Delta_c) = 1$ and $\varepsilon = f(\Delta_c) - \Delta_c$, *i.e.* at Δ_c the map has a tangent parallel to the identity and the vertical distance to the identity at this point is ε and is given by

$$\varepsilon = b_0 - \frac{(1-b_1)^2}{4b_2}. \tag{6.25}$$

In Figure 6.2 we show an example of an iteration of the map in Eq. (7.1) for a set of typical simulation parameters.
The number of iterations T needed to pass through the bottleneck between the map and the identity is of order $T = \pi/\sqrt{\varepsilon b_2}$ (see *e.g.* [51] Chap. 5). Hence we have

$$\left(\frac{\pi}{T}\right)^2 = b_0 b_2 - \frac{1}{4}(1-b_1)^2 \tag{6.26}$$

We can simplify this expression by only working to the lowest order in the killing probability and further more we will only include mutation processes considered above, *i.e.* single gene mutations in one or in both offspring. Let us denote by P_0 the probability that no mutation occur, *i.e.* $P_0 = (1-p_{mut})^{2L}$. Since we neglect all other mutation events than the two kinds just described, we have the approximation

$$1 - P_0 = (P_{mut}^{(0)} + L p_{mut}^{(1)}) L p_{mut}^{(1)}, \tag{6.27}$$

in which case Eq. (6.19) becomes

$$A = \left(\frac{k\bar{J}}{N} - \mu\right) P_0 + \left(\frac{k\tilde{J}}{N} - \mu\right)(1-P_0). \tag{6.28}$$

With these approximations we arrive at

$$\left(\frac{\pi}{T}\right)^2 \simeq -\frac{k}{2N}(\bar{J}-\tilde{J})(1-P_0)\left[\frac{k}{N}(\bar{J}-\tilde{J})P_0 + \frac{k}{N}\tilde{J} - \mu\right] p_{kill}^2. \tag{6.29}$$

We find that $kP_0(\bar{J}-\tilde{J})/N$ is very small and hence that the expression for $(\pi/T)^2$ is well approximated by

$$\left(\frac{\pi}{T}\right)^2 \simeq -\frac{k}{2N}(\bar{J}-\tilde{J})(1-P_0)\left(\frac{k}{N}\tilde{J} - \mu\right) p_{kill}^2. \tag{6.30}$$

We conclude that our mean field analysis suggests that the length of the qESS, *i.e.* the metastable quiescent epochs, is set by four mechanisms. Firstly, it is obvious that the rate of mutations $(1-P_0)$ influences the duration of the qESS: no mutations leads to no transitions and hence lead to $T = \infty$. Secondly, the rate of killing, i.e. the factor p_{kill}^2. The rate of killing is related to the rate of offspring production, since due

to the environmental coupling term $-\mu N$ in Eq. (6.2) on average there is a balance between reproduction and killing. Hence if p_{kill} decreases the rate of reproduction decreases and fewer mutations are produced leaving the qESS more stable and T larger. The third mechanism influencing T is the mismatch between the characteristic interaction strength between the set of extant types and mutant types located in the perimeter of the set of extant types, i.e. the factor $(\bar{J}-\tilde{J})$. One may consider this factor as being related to the selective pressure on the qESS state. Namely, if $\bar{J}=\tilde{J}$ there is no selective pressure, since the mutants are entirely like the wild types. The lack of selective pressure drives T to become infinite. Finally the term $k\tilde{J}-\mu$. Again one may see the fact that when $k\tilde{J}/N=\mu$ the duration T becomes infinite as representing the fact that a mutant population for which $k\tilde{/}N=\mu$ is already well tuned to the environmental pressure represented by μ.

It is of course interesting to try to relate the prediction for the duration T given by Eq. (6.30) to the actual qESS intermittency observed in simulations of the Tangled Nature model. To do this we have determined the time average values of $\bar{J}$ and $\tilde{J}$ during 4000 qESS states and plot the distributions obtained in Fig. 6.3. In order for Eq. (6.30) to make sense the sign has of course to be positive. The two terms that could in principle be problematic are $(\bar{J}-\tilde{J})$ and $(\frac{k\tilde{J}}{N}-\mu)$. In Fig. 6.3 we show the distribution of these terms obtained from a set of 4000 measured qESS. The difference in the average J's is always positive while the second term is alway negative. Given the high stochasticity of the TaNa, this doesn't mean that a specific qESS cannot produce a negative value, but that this is extremely unlikely, and perhaps it wouldn't last long enough for us to notice it. Amongst all the realisations of $\bar{J}$ and $\tilde{J}$ we recorded only 0.16% corresponds to a negative right hand side in Eq. (6.30).

Indeed one has to consider —Eq.(30) as a qualitative description of the duration more than a quantitative one. This is the case because of the approximations we were forced to make when deriving the mean field expressions. Moreover, it is difficult to relate the quantitive values for T obtained from Eq. (30) to the durations observed in the simulations because of the always difficult problem of relating mean field time to Monte Carlo simulation time steps.

Successive tangent bifurcation model

Based on the analysis in the previous section we now advance a simple nonlinear dynamical model capable of imitating some features of the macroscopic dynamics that can be typically generated by the TaNa model. It is important to notice that the local tangent map we obtained in Eq. (6.2) can only generate one qESS episode since it does not provide a reinjection mechanism or alternative continuation of dynamical evolution. Therefore, to reproduce sequences of qESS episodes it is necessary to extend this first result. We shall be guided by Eq. (6.30) to do this. This equation establishes the factors that affect the duration T of the qESS. These factors are driving forces for the hectic bursts that terminate one qESS and generate a new one. The numbers and types of species in the sequences of qESS in the TaNa model may (and do) change from one qESS to the next. This occurs at the hectic bursts. If this feature is to be reproduced the period of the attractor associated with the tangent bifurcation should have the capability to be changed. Our model considers families of chaotic attractors in the vicinity of tangent bifurcations present in low-dimensional iterated maps that display intermittency, referred to as intermittency of type I [51]. For convenience these families can be taken from those occurring an infinite number of times in unimodal maps, as represented by the quadratic logistic map, $f_\nu(x)=1-\nu x^2$, $-1\leq x\leq 1$, $0\leq\nu\leq 2$.

Unimodal maps share self-similar families of attractors such as chaotic attractors that consist of 2^k, $k=0,1,2,\ldots$, bands. For given k the 2^k-band attractors appear for a given range of the control parameter ν, with the exception of some smaller intervals where periodic attractors reappear. See Fig. 6.4. These

intervals are control parameter windows of regular behaviour that start at a tangent bifurcation at which chaotic dynamics transforms sharply into periodic motion. The dynamics at the chaotic attractors in the vicinity of the left edge, $\nu \lesssim \nu_\tau$ of the window of periodic attractors, the location $\nu = \nu_\tau$ of the tangent bifurcation, displays intermittency, *i.e.*, at $\nu \lesssim \nu_\tau$ where ν_τ is the location of the tangent bifurcation. That is, the map trajectories consist of quasi-periodic motion interrupted by bursts of irregular behaviour. The iteration time duration of the quasi-periodic episodes increases as the tangent bifurcation is approached and the statistical features of these durations have been shown to display characteristics of various types of noise [53]. At the tangent bifurcation the duration of the episodes diverges and the motion becomes periodic. The opening periods τ of the windows follow the Sharkovskii ordering [64]. A single tangent bifurcation of a unimodal map linking a fixed period attractor to a chaotic one is only capable of portraying a fixed set of types of species and a fixed total number of them, *i.e.* no evolutionary change. Whereas a set of such tangent bifurcations visited sequentially according to some rules can describe consecutive quasi-stable episodes with varying numbers of species and total population, as in a evolutionary process. The following procedure, which incorporates the criteria identified above for the duration of the qESS, can be used to generate successive quasi-periodic events of different (quasi)-periods mediated by brief erratic bursts, each event associated with a different periodicity τ_n and of different duration T_n. First choose a control parameter value ν_0 just left of a window of periodicity τ_0 of the logistic map with tangent bifurcation at ν_{τ_0}, $\delta\nu_0 \equiv \nu_0 - \nu_{\tau_0} \lesssim 0$. When the map trajectory with initial condition x_0 comes out of the bottlenecks formed by $f^{(\tau_n)}(x)$ and the identity line (see Fig. 6.2) (to experience a chaotic burst before it is re-injected close to the bottlenecks) the control parameter of the map is changed and the trajectory continues its evolution in a different environment. This change in control parameter is mediated by a set of stochastic conditions, that when fulfilled another control parameter value ν_1 is generated just left of a window of periodicity τ_1 with $\delta\nu_1 \equiv \nu_1 - \nu_{\tau_1} \lesssim 0$, and so on for $n = 2, 3, \ldots$. Two of these conditions refer to exceedances associated with two random variables δ_1 and δ_2, generated by a normal and a uniform distributions, respectively. The conditions are $\delta_1 > \Gamma_1$ and $\delta_2 > \Gamma_2$ where Γ_1 and Γ_2 are two prescribed thresholds. Samplings for δ_1 and δ_2 run until the two thresholds are overcome simultaneously a given number l of times ($l = 2$ for our results shown below). Then the control parameter value is changed to that of a different window chosen at random. The new value of $\delta\nu_n$ is estimated via $\delta\nu_n \sim (T_n)^{-2}$ (see *e.g.* [51] Chap. 5), where the duration T_n is given by Eq. (6.30). The two implemented thresholds correspond to critical values of the imbalances referred after Eq. (6.30),

$$\delta_1 = \frac{\frac{k}{N}\tilde{J} - \mu}{p_{kill}^2(1 - P_0)}$$

and

$$\delta_2 = \frac{\frac{k}{2N}(\bar{J} - \tilde{J})}{p_{kill}^2(1 - P_0)}. \tag{6.31}$$

For conciseness and clarity, in Fig. 6.5 we show as a flow diagram the algorithm followed by the consecutive tangent bifurcation model. The repetition of this prescription leads to the dynamical behavior shown in Fig. 6.6 that can be compared with that obtained from the TaNa model in Fig. 6.1. The quasi-periodic episode of period τ_n is identified with the quasi stable co-existence of n species for a time period T_n in the TaNa model and the chaotic burst at its ending leads to some extinctions and new mutated species of the following quasi-stable configuration.

This approach can be considered to be a phenomenological modelling of the original TaNa model. The threshold selections of the periodic windows τ_n at ν_{τ_n} and of the value of the control parameter distance $\delta\nu_n$ from the corresponding tangent bifurcation can be further elaborated, *e.g.* by devising specific rules

suggested by ecological principles associated with reproduction, mutation and death, and in this way obtain a closer reproduction of the dynamics of the TaNa model. Interestingly, an average decrement of the variables $\delta\nu_n$ with increasing time t, that implies an average increment of the duration of quasi-stable episodes T_n with t, observed in the TaNa dynamical properties, signals an approach to the intermittency transition out of chaos. Our modelling by means of the dynamics associated with families of tangent bifurcations implies (in a well-defined manner restricted to deterministic nonlinear dynamics) that the ecological evolution model operates near the onset of chaos, in our case, at nearly vanishing Lyapunov exponent.

The stochastic element of the model resides only in the threshold conditions to switch from the chaotic vicinity of one tangent bifurcation to the chaotic vicinity of another. The dynamical behavior of the model between these instantaneous shift times is the known chaotic deterministic dynamics in the neighborhood of tangent bifurcations of low-dimensional attractors. In the model the time duration between control parameter ν changes corresponds to the duration of the qESS (see Fig. 6.6).

To explore a possible relationship between the dynamical properties of low-dimensional nonlinear systems and the high-dimensional, and often stochastic, dynamics of relevance to complex systems it is necessary to identify a few robust macroscopic degrees of freedom of the latter that capture the salient features of its dynamical evolution. We have performed such an analysis for a particularly high-dimensional and particularly strongly stochastic model, namely, the Tangled Nature model of evolutionary ecology. We find that despite of the dramatic approximations involved in establishing a local one-dimensional map we nevertheless obtain meaningful and interesting statements concerning the duration of the long quiescent epochs of the TaNa model.

We then went on to describe how a simple quadratic map is able to reproduce structures that qualitatively exhibit, with a high degree of similarity, the full high-dimensional stochastic model. We advanced a nonlinear dynamical system model consisting of consecutive one-dimensional chaotic attractors near tangent bifurcations that generate time evolution patterns resembling those of the TaNa model in macroscopic scales. These tangent bifurcations are chosen from the infinite families that occur at the onset the periodic windows in the logistic map according to a threshold prescription based on the previously identified mechanisms that control the duration of the basic quasi-stable event generated by the local map derived from the TaNa model. These mechanisms involve imbalances between (average) values of parameters with ecological meaning that define the TaNa model. See Eq. (6.30) and text below it.

The manner into which randomness has been introduced in the consecutive tangent bifurcation model does not generate any unstable behavior in the low-dimensional intermittency. The random changes in the control parameter take place instantaneously according to the algorithm described in the previous section. Otherwise, the dynamics is fully deterministic, and follows known patterns associated with the families of tangent bifurcations in a quadratic map.

The generally unanticipated link we established between the macroscopic dynamics of a high–dimensional stochastic model and the intermittent dynamics of low-dimensional systems requires a closer examination. This can be developed, first, by deriving under less sweeping approximations the collapse of degrees of freedom that leads to this correspondence. This would include the derivation from the TaNa model of a more complete, tangent bifurcation model to fit more closely the mutual interactions that define the TaNa model of evolutionary ecology. The occurrence of the connection between high-dimensional and low-dimensional dynamical model systems offers a new path to the study of complex systems. A possible methodology to obtain, or at least to visualize, this reduction is, as attempted here, to derive from the original model via mean-field arguments a nonlinear iterated map representation, such as a coupled map lattice. This is actually the case here for the species or agents n_i of the TaNa model when described by the approximations made on the likelihood function H_i. Such macroscopic collective behavior is known

to arise in couple map lattices [65].
We evaluate the implication and outlook of an unanticipated simplification in the macroscopic behavior of two high-dimensional stochastic models: the Replicator Model with Mutations and the Tangled Nature Model (TaNa) of evolutionary ecology. This simplification consists of the apparent display of low-dimensional dynamics in the non-stationary intermittent time evolution of the model on a coarse-grained scale. Evolution on this time scale spans generations of individuals, rather than single reproduction, death or mutation events. While a local one-dimensional map close to a tangent bifurcation can be derived from a mean-field version of the TaNa model, a nonlinear dynamical model consisting of successive tangent bifurcations generates time evolution patterns resembling those of the full TaNa model. To advance the interpretation of this finding, here we consider parallel results on a game-theoretic version of the TaNa model that in discrete time yields a coupled map lattice. This in turn is represented, a la Langevin, by a one-dimensional nonlinear map. Among various kinds of behaviours we obtain intermittent evolution associated with tangent bifurcations. We discuss our results.

Game theory and intermittent dynamics in low dimension

The next step we consider is a radical simplification of the game-theoretic CML replicator-mutation equations into a one-dimensional nonlinear map. This attempt aims at probing the possible connection between the macroscopic intermittent behaviors of the above-mentioned high-dimensional models with the low-dimensional established sources of intermittency, such as the tangent bifurcation [51] with known $1/f$ noise spectra [53]. In doing so, we reduce the many-strategy game-theoretic problem to a classic version of two strategies, where one of them represents the chosen agent or species and the other assemblages all the others. Finally, we recall that a one-dimensional nonlinear dynamical model can be constructed [66] such that its time evolution consists of successive tangent bifurcations that generate patterns resembling those of the full TaNa model in macroscopic scales. The parameters in the model are based on identified mechanisms that control the duration of the basic quasi-stable event generated by a local mean-field map derived from the TaNa model [66].

Replicator model with mutations

Here we briefly present the intermittent behavior of the Replicator Model with Mutations, details of which can be found in [67]. The replicator equation [68] was introduced in evolutionary game theory in order to capture the frequency-dependent nature of the evolution process. We are interested in the limit of many strategies. Players may leave the system (say go bankrupt or extinct) or may change their strategy (mutate). This means that the number of players choosing a given strategy and the number of available strategies are in constant evolution. This version of the replicator dynamics set-up was studied by Tokita and Yasutomi in [69]. The authors focused on the emerging network properties. Here we continue this study but with an emphasis on the intermittent nature of the macro-dynamics.
The model is described in terms of a configuration vector $\mathbf{n}(\mathbf{t})$ which contains the *relative frequencies* of all the allowed d different strategies, so the components $n_i(t) \in [0,1]$ for all $i = 1,2,...,d$. A $d \times d$ payoff matrix J contains the payoffs of every pairwise combination. The matrix J is a random and fixed interaction network on top of which the replicator dynamics will evolve. Each strategy distinguishes itself from the others in its payoffs or interactions with the rest of the strategy space. We used an uncorrelated, large matrix of dimension $d \in (10^2, 10^4)$. In the initial configuration, $N_o < d$ strategies start with the same frequency $n_i = 1/N_o$ and for all the other strategies $n_i(0) = 0$. The empty strategies can become populated

only by one of the *active* strategies mutating into them. Once this happens, their frequency will evolve according to the replicator equation, Eq. (6.32), in which these newly occupied strategies interact with the active strategies which they are linkedf through the matrix J.
A time step of the replicator dynamics consists of calculating the *fitness*, $h_i(t) = \sum_j J_{ij} n_j(t)$ of each active strategy and compare it with the average fitness $\bar{h}(t) = \sum_{ij} J_{ij} n_i(t) n_j(t)$. The frequencies are updated according to

$$n_i(t+1) = n_i(t) + \left(\sum_j J_{ij} n_j(t) - \sum_{k,j} J_{kj} n_k(t) n_j(t) \right) n_i(t). \tag{6.32}$$

When the frequency of a strategy i goes below a preset extinction threshold $n_i(t) < n^{ext}$, the strategy is considered extinct and its frequency is set to zero $n_i(t+1) = 0$. Right after an extinction event the system is immediately renormalised in order to maintain the condition $\sum_i n_i(t) = 1$.
The stochastic element consists in the following updates. With probability p^{mut} each strategy mutates into another one, this is done by transferring a fraction α_{mut} of the frequency from the considered strategy to another strategy. The label of the latter strategy is chosen in the vicinity of the first by use of a normal distribution $N(i,\Delta)$ centred on label $i \in \{1,2,...,d\}$ with variance Δ with periodic boundary conditions, i.e. label $d+1$ is identified with label 1. The closer the labels of two strategies are the more likely it is for one to mutate into the other.
The systemic level dynamics is described by $\mathbf{n}(t)$ and is shown in fig.(6.7), where we present the *occupancy* plot (left panel) and the evolution of the frequencies of the single strategies (right panel).
The parameters used in the simulations are $d = 256$, $n_{ext} = 0.001$, $\alpha_{mut} = 0.01$, $p^{mut} = 0.2$ and $\Delta = 15$ and were chosen for reasons of computational performance. The meta stable states are typically characterised by two strongly occupied strategies which are surrounded by 7 to 8 "cloud" strategies. These are populated by mutations and quickly die out.

Mean Field Description

The random mutations are the only source of stochasticity in the model's dynamics. These stochastic events can make the frequency of a strategy grow as a result of inflow from different strategies mutating on to the given strategy and can lead to a strategy looses part of its frequency due to mutations onto other strategies. The gain is on average given by $\alpha_{mut} n_j(t+1)$ which happens with probability $p_{mut} \sum_{j \in N_a} p_{j \to i}$, where N_a is the number of active strategies and

$$p_{j \to i} = \frac{e^{\frac{-|i-j|^2}{2\Delta^2}}}{\sqrt{2\pi\Delta^2}} \tag{6.33}$$

is the probability of i mutating into j (and viceversa). A fraction of players α_{mut} are lost, which happens with probability p_{mut}. We therefore get the mean field description as

$$\begin{aligned} n_i(t+1) \simeq n_i(t) + & \left(\sum_j J_{ij} n_j(t) - \sum_{jk} J_{ik} n_i(t) n_k(t) \right) n_i(t) \\ & + p_{mut} \alpha_{mut} \left(\sum_j n_j(t) p_{j \to i} - n_i(t) \right). \end{aligned} \tag{6.34}$$

We now bravely reduce Eq. (6.34) to a one dimensional map intending to capture the evolution of the occupancy of a single strategy as it evolves and interact with all other strategies and arrive at

$$n(t+1) = n(t) + J_1 n^2(t) + J_2 n^3(t) + \alpha n(t). \tag{6.35}$$

Here J_1 represent the average effect of the $J_{ij}n_j(t)$ term in Eq (6.34), J_2 the effect of the $J_{ik}n_i(t)n_k(t)$ term and α sums up the effect of the last term in the equation. This mean field equation is of the same form as

$$x_{k+1} = f(x_k) = x_k + \delta x_k(1-x_k)[S + (1-T-S)x_k], \tag{6.36}$$

with $\alpha = \delta S$, $J_1 = \delta(1-T-2S)$ and $J_2 = \delta(1-T-ST)$. This map has been studied in detail in [70]. Note we have included a factor δ (omitted in [70]) to represent the size of the time step when going from Eq. (1) to Eq. (2) in Ref. [70]. Here we simply present simulations in Fig. 6.8 to demonstrate that the map can reproduce behavior very similar to the simulation of the full model.
The fact that the intermittency of the high dimensional Replicator Model with Mutations may be qualitatively related to tangent bifurcation of a one dimensional map encourage us to discuss in the next section a similar strategy of dramatic dimensional reduction for the fully stochastic Tangled Nature model. The Tangled Nature model is a model of evolutionary ecology, which studies the macro-dynamics emerging from the dynamics of individual agents, co-evolving in a web of mutual interactions. The systemic level dynamics exhibit intermittency. The model was introduced in [55, 56] and since then, the model framework has been used by several authors see *e.g.* [57–61]. A summary of some of the models features and predictions can be found in [50].

Model of successive bifurcations

A simple nonlinear dynamical model is capable of imitating some features of the macroscopic dynamics described above [66]. This model makes use of families of chaotic attractors near tangent bifurcations present in low-dimensional iterated maps that display intermittency of type I [51]. These families can be taken from those occurring in quadratic maps, such as the quadratic logistic map, $f_\nu(x) = 1 - \nu x^2$, $-1 \le x \le 1$, $0 \le \nu \le 2$. The dynamics at the vicinity $\nu \lesssim \nu_\tau$ of the tangent bifurcation at $\nu = \nu_\tau$ displays intermittency. That is, the map trajectories consist of quasi-periodic motion interrupted by bursts of irregular behaviour. The iteration time duration of the quasi-periodic episodes increases as the tangent bifurcation is approached. At the tangent bifurcation the duration of the episodes diverges and the motion becomes periodic.
A phenomenological procedure for generating successive qESS with durations obtained from the criteria given by Eq. (12) is briefly described as follows [66]. First choose a control parameter value ν_0 just left of a window of periodicity τ_0 of the logistic map with tangent bifurcation at ν_{τ_0}, $\delta\nu_0 \equiv \nu_0 - \nu_{\tau_0} \lesssim 0$. When the map trajectory with initial condition x_0 comes out of the bottlenecks formed by $f^{(\tau_n)}(x)$ and the identity line to experience a chaotic burst before it is re-injected close to the bottlenecks. The map trajectory evolves in this environment (performing one or more holdup passages and re-injections) until a set of two stochastic conditions is fulfilled, in which case another control parameter value ν_1 is generated just left of a window of periodicity τ_1 with $\delta\nu_1 \equiv \nu_1 - \nu_{\tau_1} \lesssim 0$, and so on for $n = 2, 3, \ldots$. These two conditions refer to exceedances associated with two random variables δ_1 and δ_2, distributed by a uniform and a normal distribution, respectively. The conditions are $\delta_1 > \Gamma_1$ and $\delta_2 > \Gamma_2$ where Γ_1 and Γ_2 are two prescribed thresholds. Only when the two thresholds are overcome simultaneously the control parameter value is changed to that of a different window, otherwise the trajectory remains close to the same window. The two implemented thresholds correspond to critical values of the imbalances referred after Eq. (6.30),

$$\delta_1 = \frac{\frac{k}{N}\tilde{J} - \mu}{p_{kill}^2(1-P_0)} \quad \text{and} \quad \delta_2 = \frac{\frac{k}{2N}(\bar{J} - \tilde{J})}{p_{kill}^2(1-P_0)}. \tag{6.37}$$

Depending on the threshold values one obtains different dynamical patterns. When the values of Γ_1 and Γ_2 are small only one or at most a few bottleneck passages take place before there is a change of periodic window. When these values are large the number of bottleneck passages is large before there is a change in periodic window, an indication that the system is robust to environmental variations. The dynamical properties of the model are sensitive to the imbalances represented by δ_1 and δ_2 and this sensitivity represents evolutionary changes. The repetition of this prescription leads to the dynamical behavior shown in Fig. 6.9 that can be compared with that obtained from the TaNa model in Fig. 6.1. The quasi-periodic episode of period τ_n is identified with the quasi stable co-existence of n species for a time period T_n in the TaNa model and the chaotic burst at its ending leads to some extinctions and new mutated species of the following quasi-stable configuration.

Conclussions

We have considered two related high-dimensional model systems designed to represent evolving ecological systems where agents or strategies are species that undergo reproduction, death or mutation. One of them, the TaNa model is a fully stochastic model, whereas the other, a game-theoretic adaptation of the former, contains both deterministic and stochastic elements. Both models have been shown to display non-stationary intermittent behavior on macroscopic (many individual generation) time scales. Given that these model systems show macroscopic collective behavior reminiscent of low-dimensional nonlinear intermittency, we have attempted to extract from them expressions for simple nonlinear iterated maps by introducing approximations. The resulting low-dimensional dissipative maps display attractors associated with intermittency near tangent bifurcations.

The successive simplifications that have been introduced in modeling high-dimensi-onal complex systems and in exploring their properties follow this scheme: First, the TaNa model was built up by selecting simple mechanisms at the individual level for ecosystem evolution such as annihilation, reproduction and mutation to define basic time steps, and then time evolution lets these contribute to form more complicated interactions at the systems level. Second, the time evolution equations of a mean-field deterministic approximation of the TaNa model suggest a game-theoretic interpretation that leads to a replication-mutation model that preserves the non-stationary intermittent behavior for the macroscopic evolution, but permits considerations in the game theory language of strategies and pay-off values. Third, in discrete time space the replication-mutation model becomes a CML with stochastic terms so that the characteristics of the nonlinear maps that constitute it can be inspected. And finally, the latter problem was seen to represent a two-strategy symmetric game that within a time-discrete version constitutes a one-dimensional map with two control parameters. This was recognized [70] as a replicator bimodal map that displays the routes to chaos familiar in unimodal maps that display period doublings, chaotic attractors and intermittency.

Therefore, pending stricter analysis, we preliminarily identify the macroscopic behavior of the high-dimensional model systems we describe here as composed of (effective) low-dimensional intermittency. The remarkable collapse of degrees of freedom that this circumstance entails may turn out to be more general than the few instances in which similar conduct has previously been encountered [65, 71]. This prospect, and the advance in understanding it delivers, promotes a revitalization of a close relation between nonlinear dynamical theory and the science of complex systems.

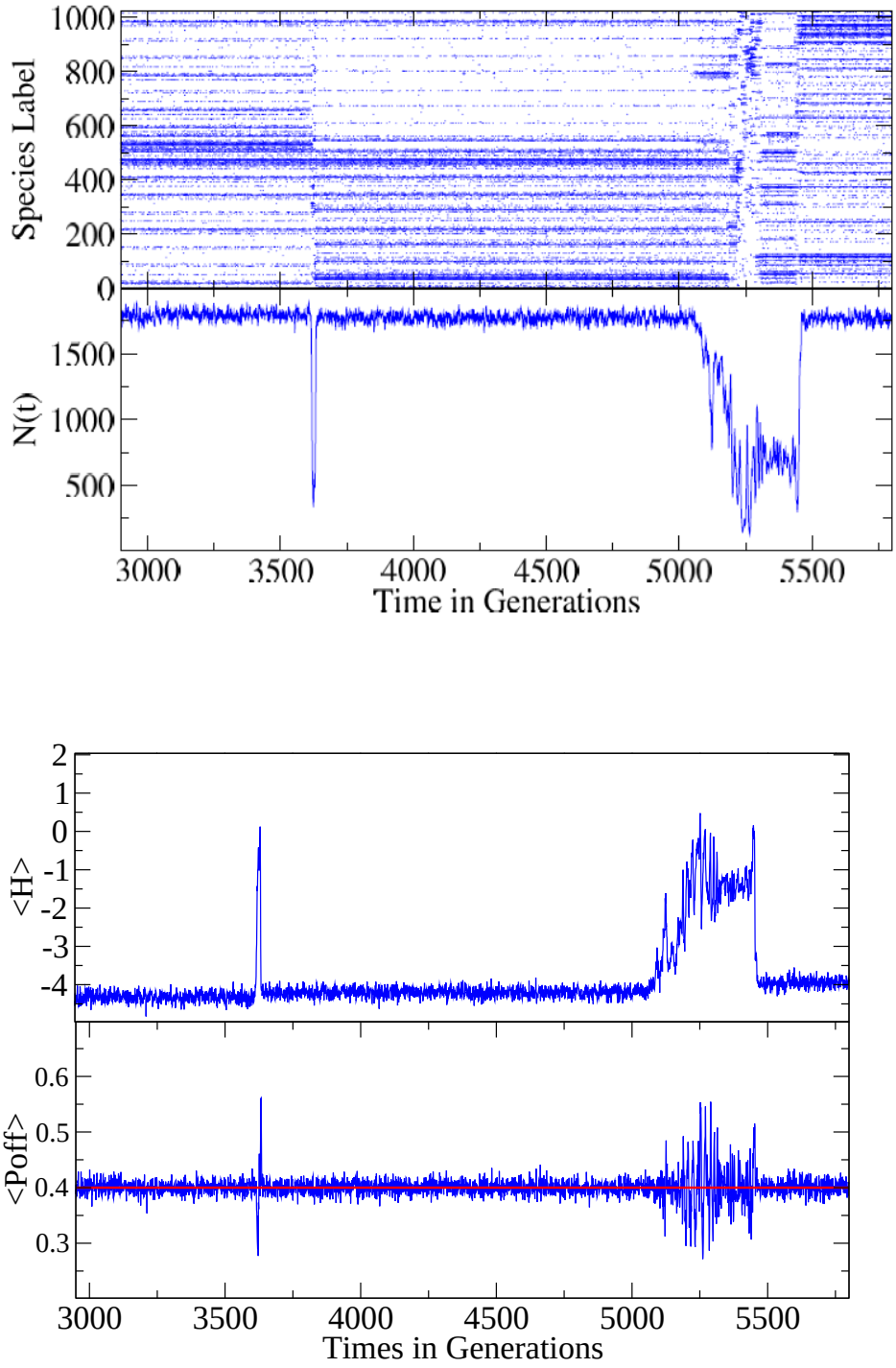

Figure 6.1: Upper Panel: Total population as a function of time (in generations) for a single realization of the TaNa model. The punctuated dynamics is clearly visible: quasi-stable periods alternate with periods of hectic transitions, during which $N(t)$ exhibits large amplitude fluctuations. Lower panel: The average of the weight function H and the reproduction probability. The parameters are $L = 10$, $p_{kill} = 0.4$, $p_{mut} = 0.02$, $\mu = 0.007$, $k = 40$ the red line indicates p_{kill}.

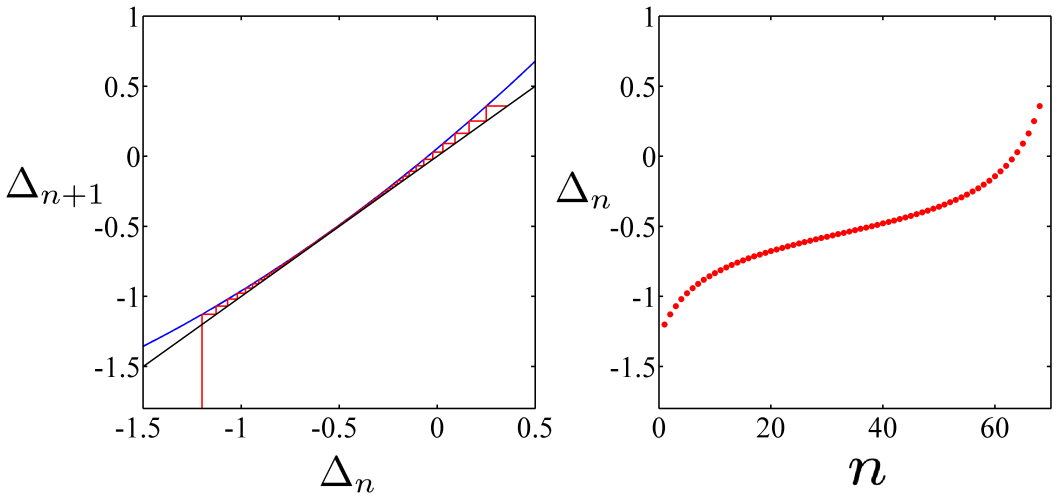

Figure 6.2: The left panel shows the first 67 iterations of the map in Eq. (7.1), with initial condition $\Delta_0 = -1.2$. The corresponding trajectory is shown in the right panel. The set of parameter values is the same than that as for Fig. 6.1, with the corresponding averaged interactions $\bar{J} \approx 0.0587$ and $\tilde{J} \approx -0.000001$, thus yielding the coefficients of the map $b_0 \approx 0.060784$, $b_1 \approx 1.167990$ and $b_2 \approx 0.151191$.

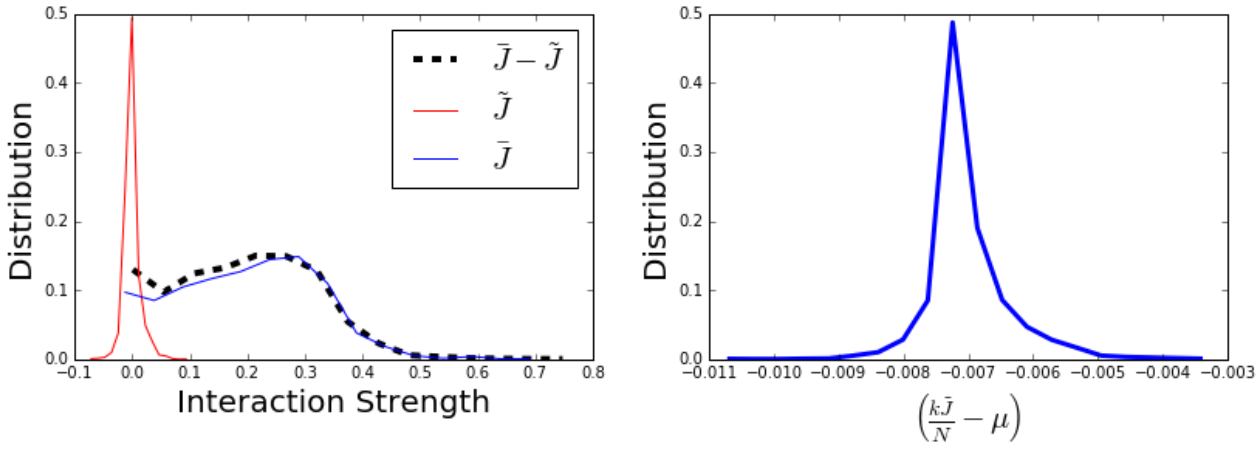

Figure 6.3: The distribution of factors that enter into the expression Eq. (6.30) for the duration of the qESS. The $\bar{J}$ and $\tilde{J}$ are the time averaged during a qESS. The data show is sampled over 4000 qESS realisations. The parameters for the simulation is the same as in Fig. 6.1

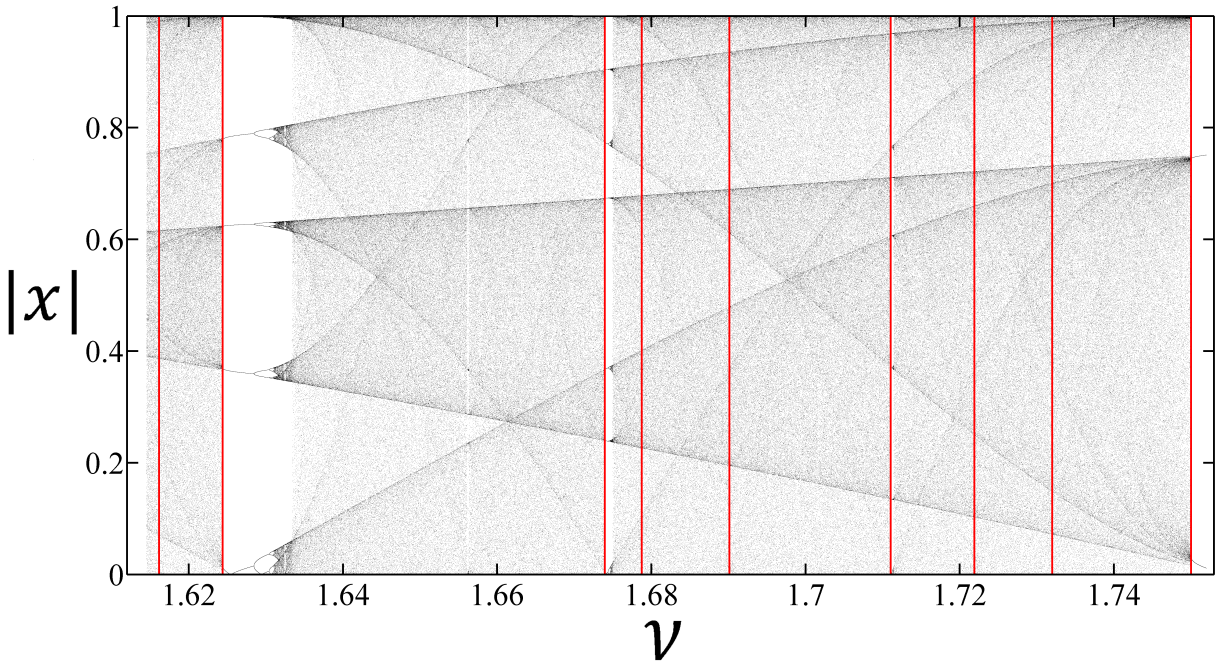

Figure 6.4: Families of chaotic attractors with interspersed periodic attractor windows for the logistic map with positions in absolute values, for a range of control parameter values ν. The red lines indicate the control parameter values that correspond to the segments appearing in Fig. 6.6. The periods associated with the vertical red lines are, from left to right, 5, 7, 12, 9, 8, 10, 11 and 3.

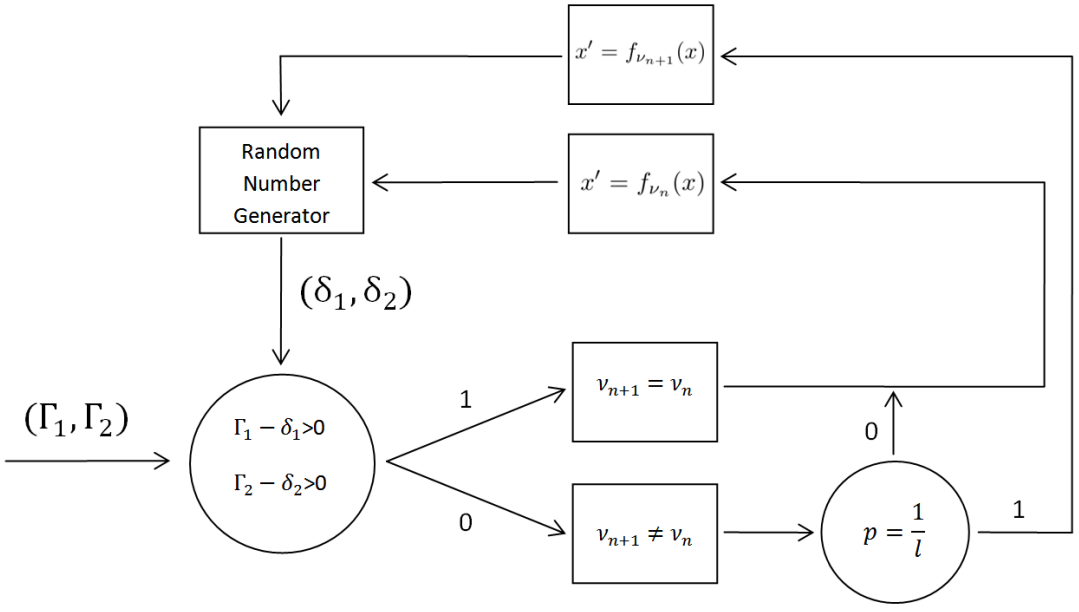

Figure 6.5: Schematic flow diagram of the algorithm under which the consecutive tangent bifurcation model operates. The successive values of $\delta\nu_n$ are estimated via $\delta\nu_n \sim (T_n)^{-2}$. We have used $l = 2$ for our numerical results. See text for description.

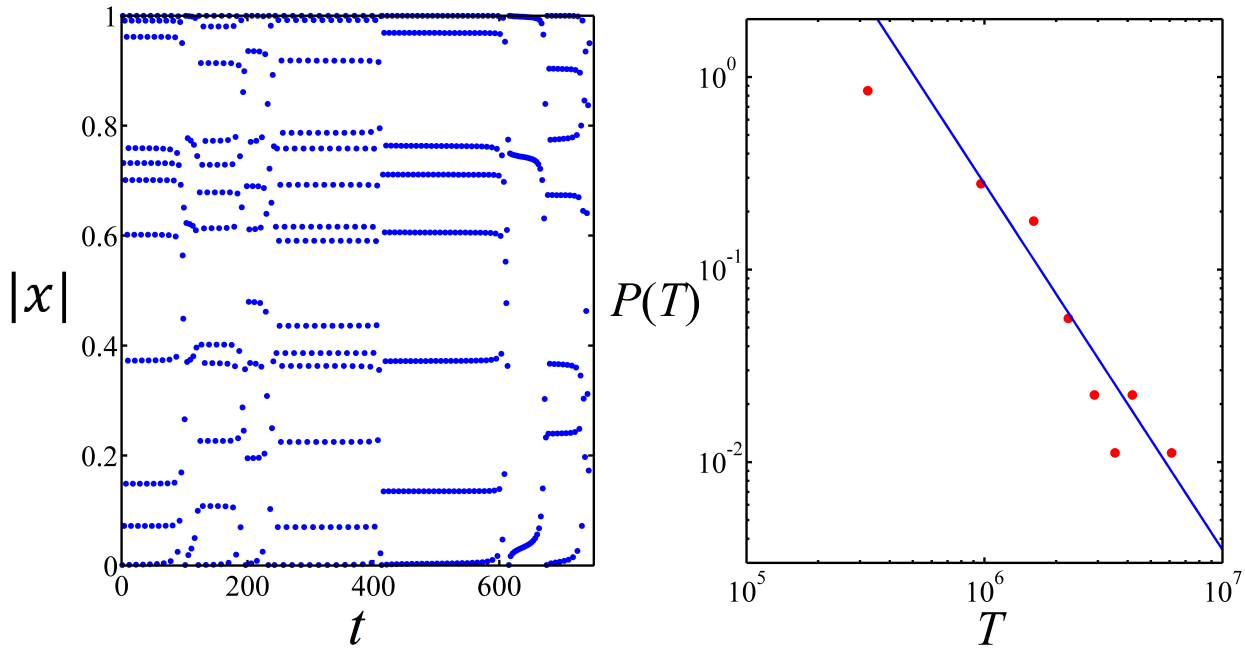

Figure 6.6: Left Panel: Iterated time t evolution of a trajectory generated by the consecutive tangent bifurcation model. The figure is composed of segments, each of which corresponds to a fixed value of the control parameter ν_n close to a tangent bifurcation of a given period τ_n. The periods of the segments are consecutively, from left to right, 11, 5, 12, 9,... Positions appear in the figure in absolute values. Iteration times t would correspond to generations in the TaNa model (as in left panel in Fig. 1). Right Panel: Log-Log plot of the distribution of durations T of the quasi stationary episodes near the tangent bifurcations of the phenomenological model. It approximates a power law with exponent -1.87 that resembles the distribution of qESS episodes obtained from simulations of the TaNa model in Ref. [6].

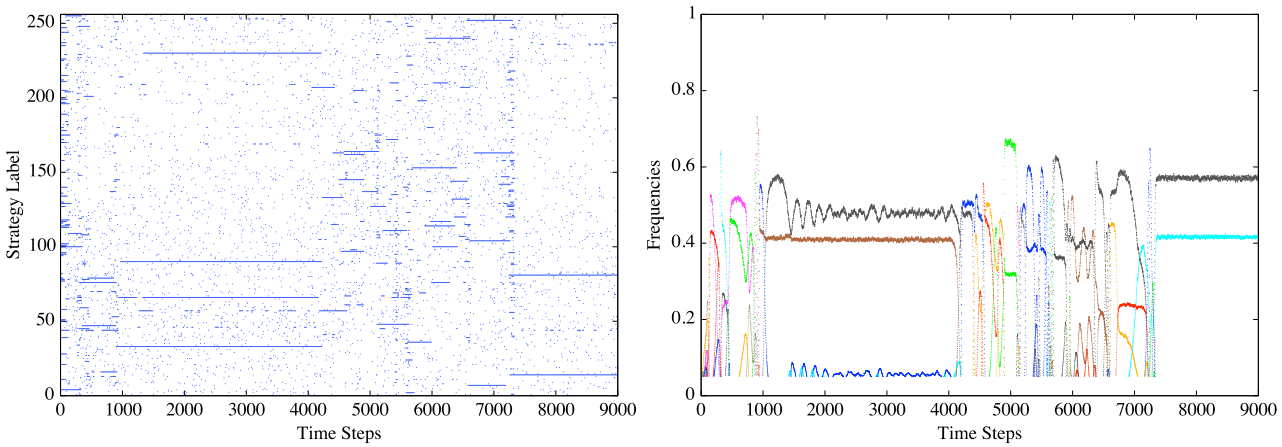

Figure 6.7: Left panel: occupancy distribution of the types. The genotypes are labelled arbitrarily and a dot indicates a type which is occupied at the time t (*i.e.* $\mathbf{n}(t) > 0$). The punctuated dynamics is clearly visible: quasi-stable periods alternate with brief periods of hectic transitions. Right panel: the frequencies of the strategies. Each colour belongs to a different strategy. Once again the transitions from one meta stable configuration (approximate fixed point) to another is clear.

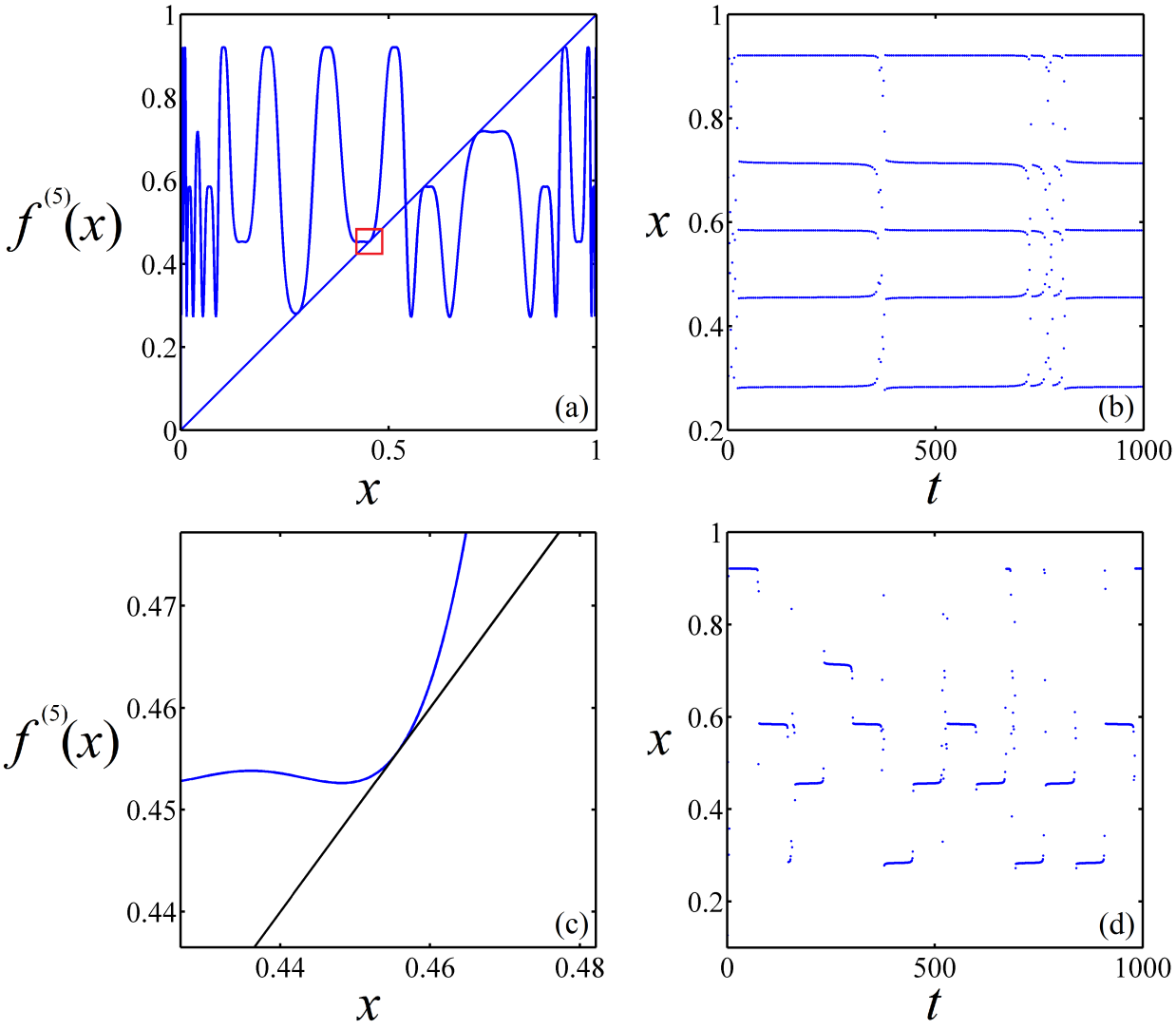

Figure 6.8: Simulation of the replicator map in Eq. (6.36) near a period five periodic window with control parameters $S = T = 6.5950$. Panel (a): The map (Eq. (6.36)) composed five times. Panel (b): Trajectory obtained from the map without being composed, $f(x)$, showing the laminar episodes separated by chaotic bursts. Panel (c): Enlargement of the map in (a) showing a local near-tangent piece. See the enclosed region inside the square in Panel (a). Panel (d): Trajectory obtained form the map $f^{(5)}(x)$ showing the laminar episodes separated by chaotic bursts. The value of the Lyapunov exponent is $\lambda = 0.001391$.

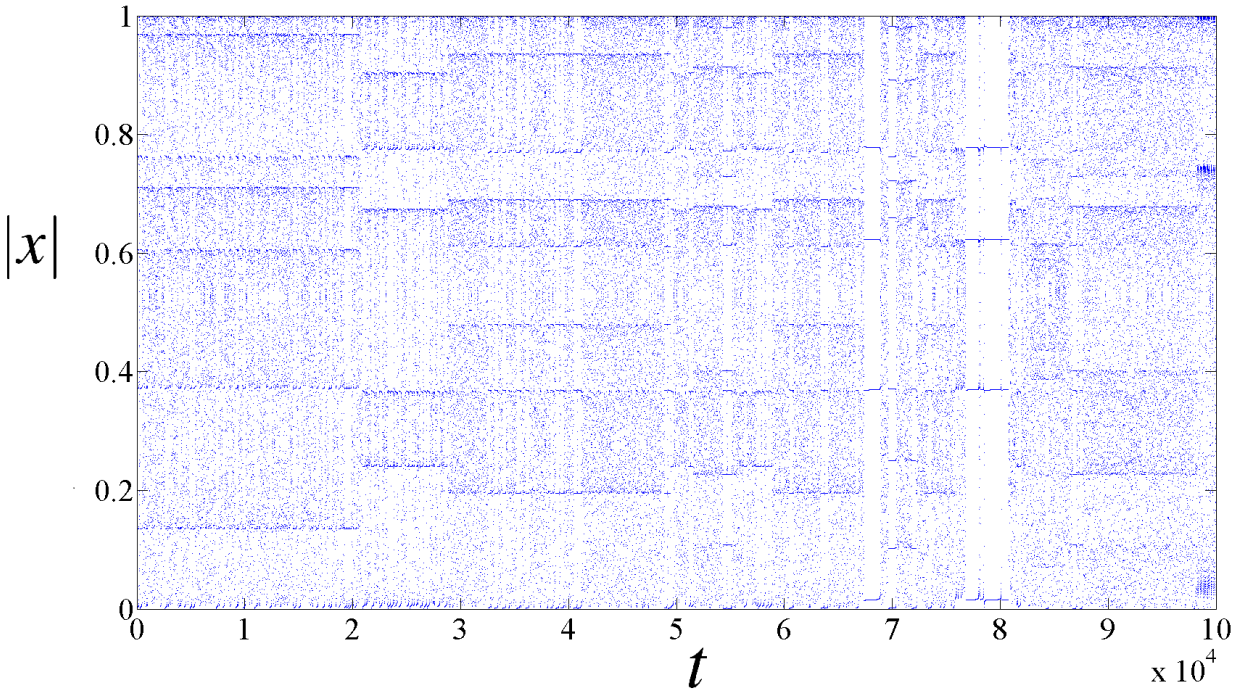

Figure 6.9: Iterated time evolution of a trajectory generated by the consecutive tangent bifurcation model. The figure is composed of segments, each of which corresponds to a fixed value of the control parameter close to a tangent bifurcation, associated with a given period. Within each segment, many laminar episodes occur separated by chaotic bursts. The periods of the segments are consecutively, from left to right, 8, 7, 9,... Positions appear in the figure in absolute values.

Part IV

Summary and Discussion

Chapter 7

Effective behavior in the studied models

In this last chapter, most important results are summarized. As a brief discussion some commentaries regarding those results are added, and some conjectures I consider valuable for rounding this document are made. Perhaps these conjectures result to be interesting for future works.

Hence, it is sensible to recall the main items stated in the exposed works:

1. We found low-dimensional dynamical behavior whose statistical description corresponds to long-standing, quasi-stable crossover distributions existing between gaussian and singular distributions.

2. The loss of correlations between deterministic variables close to the accumulation point of a bifurcation cascade implies the validity of the central limit theorem, for dynamics arbitrarily close to this accumulation point.

3. After applying strong assumptions leading to a mean field calculation over a high-dimensional model for ecological evolution, we obtained a one-dimensional map close to a tangent bifurcation which exhibits intermittent behavior. With use of the theory on $1/f$ noise developed by Procaccia and Schuster, we are able to calculate the laminar periods from the parameters of the original TaNa.

4. At the level of the dynamics of population in terms to the replicator equation for each of the species of the model, after preforming an approximation we get again a map exhibiting type-I intermittency.

5. We studied a dissipative, one-dimensional map for two subsequences of values of its control parameter. We followed the evolution of the density of an initial uniform ensemble of trayectories and calculated the corresponding entropy with the Shannon expression. A phase transition occurs in terms of the thermodynamic (Shannon) entropy, related to a change in the invariant measure induced by the dynamics of the map.

Some commentaries are in order regarding points 1 and 2. It has been clear since long ago [42] that mixing is lost at the accumulation point of a bifurcation cascade. As a little accomplishment, here we give more formal evidence on what until now has only been conjectured and claimed everywere: That ergodicity is at this point is necessarily also missing. This assumption has been instrumental in many works concerning the supposed generalizations of statistical mechanics via Tsallis claims.

Effective degrees of freedom and coarse graining

Points from 3 to 5 can be discussed in terms of the concept of coarse-graining. Coarse-graining is necessary for building models of nature. Every time we construct a model we are coarse-graining our observations by reducing the number of variables or the level of detail in the description. This is specially true for complex systems. As an example, we take the Tangled Nature Model of evolutionary ecology, fully explained in Part III, that carries with it a heavy coarse graining of the real process of ecological evolution. As a critique to this model it must be said that it does not incorporate factors considered as fundamental for the evolution of the great mayority of ecological systems, such as the interaction of members of a species with themselves, among other considerations that are perhaps more subtle to be treated in this brief conclussion of my work. Correspondingly, the assumptions made in [66, 72] to derive the mean field map

$$\Delta_{n+1} = b_0 + b_1\Delta_n + b_2\Delta_n^2 \equiv f(\Delta_n), \tag{7.1}$$

even if reasonable and based on physical intuition about ecology but are rather strong mathematically. The main assumption is that typical events exist in the space of all possible realizations of the model, such that a change in the dynamics of the main function H due to a microscopic event (or perturbation), is guaranteed with probability p. This in turn implies that the impact of the species on the macroscopic dynamics is homogeneous, which is by no means obvious, on the contrary, it is a strong assumption. And not only mathematically, it also sounds counterintuitive for an ecologist. Is in that spirit that further analysis can be performed, assuming some inhomogeinity in the impact of the species. There are other pending explorations, such as an thorough analysis of the regions on parameter space of the TaNa model on which this intermittent behavior is allowed to happen [*].
There is another peculiar occurrence of coarse-graining in our work, that I would consider as 'induced' or natural rather than imposed by some fine-tuned criteria. This is what points 1, 2 and 5 are special about. According to our findings, there is a separation of time scales: that of the time iteration of the transformation f (we also used T) and such that the action of the Frobenius-Perron operator is invariant. This is not an isolated fact, but a consequence of the underlying dynamics of the map close and on the accumulation point of the bifurcation cascade. The dynamics on these points becomes fractalized due to the structure of the attractors, that are actually successive steps on the construction of a Cantor set of infinite scales. The existence of this time scale and of a 'quasi-stationary' state for the action of the Frobenius-Perron operator strongly suggests that there is some level of coarse graning on the system due to two main facts that I have identified. First, that finite precision of any numerical calculation prevents the finest description to be achieved, then, in this sense is that the coarse-grained is induced in the first place. Second, the separation of time scales invites to think that, among all the different regions on the interval of definition of the transformation f, there begins to emerge a special set of them that are of particular importance when we see the system in a collective way, by iteratin ensembles of positions and not only observing isolated trajectories.

It is that inspired by those findings and conjectures that I think we can little by little construct a general theory of complex systems. Perhaps a general understanding and classification of complex systems can be done if we make the proper questions with the aid of the proper and modern mathematical tools.

[*] I want to thank Hugo Hernández for pointing this in our useful discussions.

Bibliography

[1] C. Lanczos. *The variational principles of mechanics*. Dover Publications Inc., New York, 1970.

[2] L. Boltzmann. *Lectures on Gas Theory*. Dover Publications Inc., New York, 2015.

[3] J. W. Gibbs. *Elementary Principles in Statistical Mechanics*. Dover Publications Inc., New York, 2018.

[4] M. O. Hill. Diversity and evenness: A unifiying notation and its consequences. *Ecology*, 54:427–432, 1973.

[5] K. Huang. *Lectures on statistical physics and protein folding*. 2005.

[6] M. E. J. Newman. The structure and function of complex networks. *SIAM Review*, 45:167, 2003.

[7] S. H. Strogatz. Exploring complex networks. *NATURE*, 410:167, 2001.

[8] J. Brown. *Ergodic Theory and Topological Dynamics*. Academic Press, 1976.

[9] J. L. Lebowitz. Modern ergodic theory. *Physics Today*, 26(2):23–29, 1973.

[10] N. S. Krylov. *Works on the foundations of statistical physics*. Princeton University Press, 1979.

[11] T. Hill. *An introduction to Statistical Thermodynamics*. Dover Publications Inc., New York, 1986.

[12] J. A. Lázaro Camí. *Ergodic Theory (Lecture Notes)*. 2010.

[13] S. Sternberg. *Dynamical Systems*. Dover Publications Inc., New York, 2010.

[14] J. Albarrán. *A guide to the Ergodic Decomposition Theorem: Ergodic Measures as Extreme Points*. 2004.

[15] T. Pereira. *Introduction to Ergodic Theory (Lecture Notes)*. 2013.

[16] A. Lasota and J. A. Yorke. Exact dynamical systems and the Frobenius-Perron operator. *Transactions of the American Mathematical Society*, 48:375, 1982.

[17] R. M. May. Simple mathematical models with very complicated dynamics. *Nature*, 262:459–67, 1976.

[18] S. van Strien and W. de Melo. *One-dimensional dynamics*. 1992.

[19] C. Preston. *Lecture Notes on Mathematics: Iterates of piecewise monotone mappings on an interval*. Springer-Verlag, 1988.

[20] J.-P. Eckmann. Ergodic theory of chaos and dynamical systems. *Reviews of Modern Physics*, 57 Part I:617, 1985.

[21] A. Robledo. Generalized statistical mechanics at the onset of chaos. *Entropy*, 15:5178, 2013.

[22] L.G. Moyano and A. Robledo. q-deformed statistical-mechanical property in the dynamics of trajectories en route to the Feigenbaum attractor. *Physical Review E*, 77:036213, 2008.

[23] A. Diaz-Ruelas and A. Robledo. Emergent statistical-mechanical structure in the dynamics along the period-doubling route to chaos. *Europhysics Letters*, 105:40004, 2014.

[24] M. A. Fuentes and A. Robledo. Renormalization group structure for sums of variables generated by incipiently chaotic maps. *Journal of Statistical Mechanics*, 2009.

[25] A. Robledo M. Fuentes. Sums of variables at the onset of chaos. *Eurpean Physical Journal B*, 87:32, 2014.

[26] A. Díaz-Ruelas, M. A. Fuentes, and A. Robledo. Scaling of distributions of sums of positions for chaotic dynamics at band-splitting points. *Europhysics Letters*, 108:20008, 2014.

[27] A. Diaz-Ruelas and Alberto R. Sums of variables at the onset of chaos, replenished. *European Physical Journal: Special Topics*, 225(13-14):2763–2769, 2016.

[28] A. Diaz-Ruelas and A. Robledo. Scaling of distributions of sums of positions for chaotic dynamics at band-splitting points. *Europhysics Letters*, 108:20008, 2014.

[29] A. Diaz-Ruelas and A. Robledo. Sums of variables at the onset of chaos, replenished. *Eurpean Physical Journal: Special Topics*, 225:2763–2769, 2016.

[30] P. Cvitanovic, R. Artuso, R. Mainieri, G. Tanner, and G. Vattay. *Chaos: Classical and Quantum*. chaosbook.org, 2018.

[31] M. A. Fuentes and A. Robledo. Renormalization group structure for sums of variables generated by incipiently chaotic maps. *Journal of Statistical Mechanics: Theory and Experiment*, 2010(01):P01001, jan 2010.

[32] M. A. Fuentes and A. Robledo. Stationary distributions of sums of marginally chaotic variables as renormalization group fixed points. *Journal of Physics: Conference Series*, 201:012002, jun 2010.

[33] U. Tirnakli, C. Beck, and C. Tsallis. Central limit behavior of deterministic dynamical systems. *Physical Review E*, 75(4):040106, apr 2007.

[34] U. Tirnakli, C. Tsallis, and C. Beck. Closer look at time averages of the logistic map at the edge of chaos. *Physical Review E*, 79(5):056209, may 2009.

[35] P. Grassberger. Proposed central limit behavior in deterministic dynamical systems. *Physical Review E*, 79(5):057201, 2009.

[36] O. Afsar and U. Tirnakli. Generalized Huberman-Rudnick scaling law and robustness of q-Gaussian probability distributions. *Europhysics Letters*, 101(2):20003, jan 2013.

[37] O. Afsar and U. Tirnakli. Relationships and scaling laws among correlation, fractality, Lyapunov divergence and q-Gaussian distributions. *Physica D: Nonlinear Phenomena*, 272:18–25, 2014.

[38] C. Tsallis S. Umarov and S. Steinberg. On a q-central limit theorem consistent with nonextensive statistical mechanics. *Milan Journal of Mathematics*, 76:307, 2008.

[39] M. Gell-Mann R. Hanel, S. Thurner. Generalized entropies and the transformation group of superstatistics. *Proc. Natl. Acad. Sci. USA*, 108:6390, 2011.

[40] U. Tirnakli and E. P. Borges. The standard map: From Boltzmann-Gibbs statistics to Tsallis statistics. *Nature Publishing Group*, pages 2–9, 2015.

[41] B. A. Huberman and J. Rudnick. Scaling Behavior of Chaotic Flows. *Physical Review Letters*, 45(3):154–156, 1980.

[42] H.G. Schuster and W. Just. *Deterministic Chaos. An Introduction*. VCH Publishers, Weinheim, 1988.

[43] C. Beck and F. Schlogl. *Thermodynamics of Chaotic Systems*. Cambridge University Press, Cambridge, 1993.

[44] C. Grebogi, E. Ott, and J. A. Yorke. Crises, sudden changes in chaotic attractors, and transient chaos. *Physica D: Nonlinear Phenomena*, 7(3):181–200, 1983.

[45] W. Feller. *An Introduction to Probability Theory and its Aplications, Vol. II, 2nd ed.* John Wiley & Sons, New York, 1971.

[46] C. Tsallis. *Introduction to Nonextensive Statistical Mechanics: Approaching a Complex World.* Springer, 2009.

[47] M. De Groot. *Probability and Statistics*. Addison-Wesley Publishing Company, 1986.

[48] C. Tsallis A. M. C. de Souza. Student's t- and r-distributions: Unified derivation from an entropic variational principle. *Physica A*, 236:52, 1997.

[49] I. Procaccia and H.G.Schuster. Functional renormalization-group theory of universal 1/f noise in dynamical systems. *Physical Review A*, 28:1210, 1983.

[50] P. Sibani and H. J. Jensen. *Stochastic Dynamics of Complex Systems*. Imperial College Press, 2013.

[51] H.G. Schuster and W. Just. *Deterministic Chaos. An Introduction*. Wiley-VCH Publishers, 2005.

[52] B. Hu and J. Rudnick. Exact solutions to the Feigenbaum Renormalization-Group equations for intermittency. *Physical Review Letters*, 48:1645, 1982.

[53] I. Procaccia and H.G.Schuster. Functional renormalization-group theory of universal 1/f noise in dynamical systems. *Physical Review A*, 28:1210, 1983.

[54] Y. Pomeau and P. Manneville. Intermittent transition to turbulence in dissipative dynamical systems. *Communications in Mathematical Physics*, 74:189–197, 1980.

[55] K. Christensen, S. A. di Collobiano, M. Hall, and H. J. Jensen. Tangled nature model: A model of evolutionary ecology. *Journal of Theoretical Biology*, 216:73–84, 2002.

[56] M. Hall, K. Christensen, S. A. di Collobiano, and H. J. Jensen. Time-dependent extinction rate and species abundance in a tangled-nature model of biological evolution. *Physical Review E*, 66, 2002.

[57] P. A. Rikvold and R. K. P. Zia. Punctuated equilibria and 1/f noise in a biological coevolution model with individual-based dynamics. *Physical Review E*, 68, 2003.

[58] R. K. P. Zia and P. A. Rikvold. Fluctuations and correlations in an individual-based model of evolution. *Journal of Physics A: Mathematical and General*, 37:5135–5155, 2004.

[59] N. Becker and P. Sibani. Evolution and non-equilibrium physics: A study of the tangled nature model. *Europhysics Letters*, 105:18005, 2014.

[60] A. E. Nicholson and P. Sibani. Cultural evolution as a nonstationary stochastic process. *Complexity*, 2015.

[61] P. Vazquez, J.A. del Rio, K.G. Cedano, M. Martinez, and H. J. Jensen. An entangled model for sustainability indicators. *PLoS ONE*, 10:e0135250, 2015.

[62] P. G. Higgs and B. Derrida. Genetic distance and species formation in evolving populations. *Journal of Molecular Evolution*, 35(5):454–465, 1992.

[63] J. Maynard Smith. *Evolution and the Theory of games*. Cambridge University Press, 1982.

[64] M. Schroeder. *Fractals, Chaos, Power Laws: Minutes from an Infinite Paradise*. Freeman, 1991.

[65] H. Chaté and P. Manneville. Emergence of effective low-dimensional dynamics in the macroscopic behaviour of coupled map lattices. *Europhysics Letters*, 17:291, 1992.

[66] A. Diaz-Ruelas, H. J. Jensen, D. Piovani, and A. Robledo. Tangent map intermittency as approximate analysis of intermittency in a high dimensional fully stochastic dinamical system: The tangled nature model. *CHAOS*, 26:123105, 2016.

[67] D. Piovani, J. Grujić, and H. J. Jensen. Linear stability theory as an early warning sign for transitions in high dimensional complex systems. *Journal of Physics A: Mathematical and Theoretical*, 49(29), 2016.

[68] P. D. Taylor and L. B. Jonker. Evolutionary stable strategies and game dynamics. *Mathematical Biosciences*, 40(1):145–156, 1978.

[69] K. Tokita and A. Yasutomi. Emergence of a complex and stable network in a model ecosystem with extinction and mutation. *Theoretical Population Biology*, 63:131–146, 2003.

[70] D. Vilone, A. Robledo, and A. Sánchez. Chaos and unpredictability in evolutionary dynamics in discrete time. *Physical Review Letters*, 107:038101, 2011.

[71] E. Ott and T. M. Antonsen. Low dimensional behavior of large systems of globally coupled oscillators. *CHAOS*, 18:037113, 2008.

[72] A. Diaz-Ruelas, H. J. Jensen, D. Piovani, and A. Robledo. Relating high dimensional stochastic complex systems to low dimensional intermittency. *European Physical Journal: Special Topics*, 226:341–351, 2017.